이학박사 학위논문

장 내 항상성 및 암 형성에서의

AIMP2 의 기능 연구

Studies on the role of AIMP2

in intestinal homeostasis and tumorigenesis

2017 년 2 월

서울대학교 자연과학대학원

생명과학과 생명과학전공

염 민 규

Abstract

Studies on AIMP2

in intestinal homeostasis and tumorigenesis

Min Kyu Yum

School of Biological Sciences

The Graduate School

Seoul National University

Wnt/β-catenin (CTNNB1) signaling is crucial for the proliferation and maintenance of intestinal stem cells (ISCs). In the absence of Wnt/β-catenin signaling, the ISCs undergo immediate apoptosis and subsequently the whole intestinal crypt degenerates. The ISCs niche, Paneth and Cryptal mesencymal cells secrete abundant Wnt ligands at the crypt base. However, excessive activation of Wnt/β-catenin signaling leads to ISC expansion and eventually colorectal cancer. Thus, negative regulators are required to maintain optimal levels of Wnt/β-catenin signaling.

Colorectal cancer is the third most common cancer and second leading cause of cancer-related death worldwide. Early diagnosis enables a person with cancer to receive treatment. In order to help in treating the disease, it is important to understand the early events of colorectal cancer. Because it is known that the ISCs are origin of colorectal cancer and their expansion is one of the earliest events in tumorigenesis, understanding molecular mechanisms that controls the size of ISC compartment and eventually the tumor incidence is essential.

Aminoacyl-tRNA synthetase interacting multifunctional proteins (AIMPs) function in protein synthesis as housekeepers. They stabilize the assembly of Aminoacyl-tRNA synthetases into the multi-tRNA synthetase which is macromolecular enzyme that attach specific amino acids to their corresponding tRNAs. Besides their housekeeping function in amino-acylation, the AIMPs have been implicated in signaling cascades affecting angiogenesis, immunity and apoptosis. Recently, it has also been reported that these AIMPs are associated with signaling pathways relevant to cancers.

In this study, I investigated the relationship between AIMP2 and Wnt/β-catenin signaling in a murine model of intestinal homeostasis and tumorigenesis. Hemizygous deletion of *Aimp2* resulted in enhanced Wnt/β-catenin signaling, increased proliferation of cryptic epithelial cells and expansion of ISC compartments. In an $Apc^{Min/+}$ background, *Aimp2* hemizygosity increased adenoma formation. Mechanistically, AIMP2 disrupted the

interaction between AXIN and Dishevelled-1 (DVL1) to inhibit Wnt/β-catenin signaling by competing with AXIN. Furthermore, AIMP2 inhibited intestinal organoid formation and growth by suppressing Wnt/β-catenin signaling in an AIMP2 dosage-dependent manner. Collectively, our results showed that AIMP2 acts as a haploinsufficient tumor suppressor that fine-tunes Wnt/β-catenin signaling in the intestine, illuminating a novel role for the regulation of ISC abundance and activity.

Key words: Intestinal homeostasis; Dishevelled; Colon cancer; Lgr5; Organoid

Student ID: 2011-20342

CONTENTS

LIST OF FIGURES

BACKGROUND

Anatomy and function of intestine

The digestive track is a center of the digestive system where each part has distinct functions assigned. Their key role is to digest the food into the basic nutrients or molecules as it can be absorbed into our body. Gastro-intestinal tract is the major part of the digestive tract which consists of the stomach, small and large intestine. The small intestine can be divided into three segments; the duodenum, the jejunum and the ileum. A sheet of intestinal epithelial cells at the luminal surface of the small intestine forms two unique structure called the villi and the crypts of Lieberkühn. The finger-like projections of the villi maximize surface area for efficient absorption of digested nutrients. The microvilli on the luminal side of intestinal epithelial cells further increase the surface area. The crypts of Lieberkühn where the intestinal stem cells (ISCs) reside consistently generate all the differentiated cells up to villi. Beneath epithelial layer, the fibroblasts surround and support the epithelial cell. Smooth muscle wraps around both the epithelial and stromal compartments, which is responsible for the peristaltic movement of the intestine (Fig. 1*A*).

The intestinal epithelium

The intestinal epithelium continuously self-renews every three to five days through its highly

proliferative compartment, the crypt of Lieberkühn. Within the crypt, transit amplifying progenitors divide four to five times, and its progenies differentiate and migrate up along the crypt-villus axis (Barker et al., 2008). Four main types of differentiated cells forms intestinal epithelium; the enterocytes, the goblet cells, the enteroendocrine cells, the Paneth cells (Fig. 1*B*). The enterocytes are the absorptive cells responsible for nutrient uptake. They are the major population of the differentiated cells found in the villi and tightly packed together. This close cell-to-cell adhesions forms the epithelial barrier which prevent harmful microbes from entering into the bloodstream. The goblet cells produce mucin, the major lubrication of the intestinal epithelium. The mucin attenuates the mechanical stress from food movement and inhibits bacterial colonization along the gut tube. The goblet cells mainly reside in the distal part of the intestine and are located in the villus. The enteroendocrine cells are rare population compared to the other types of cells but are found throughout the whole gatro-intestinal track. They support gastro-intestinal function by secreting hormones, and constitute enteric-endocrine system. The Paneth cells are long-lived cells (almost 50 days), exclusively located at the base of the crypt. In contrast to the other types of cells, they migrate back down the crypt-villus axis (Clevers and Bevins, 2013). They secrete a various anti-bacterial peptides such as Defensins, and express a range of signaling stimulus which support the tissue maintenance such as Wnt3a and Notch ligand, Dll4 (Sato et al., 2011). Importantly, the Paneth cells directly contact with ISC and are major constituent of ISC niche.

Figure 1. Anatomy of intestinal epithelium (A) Haematoxylin and Eosin staining of adult small intestine. (B) During homeostasis, multipotent $Lgr5^{+}$ stem cells drive regular epithelial renewal. They constantly generate secretory and enterocyte progenitor, which give rise to terminally differentiated cells

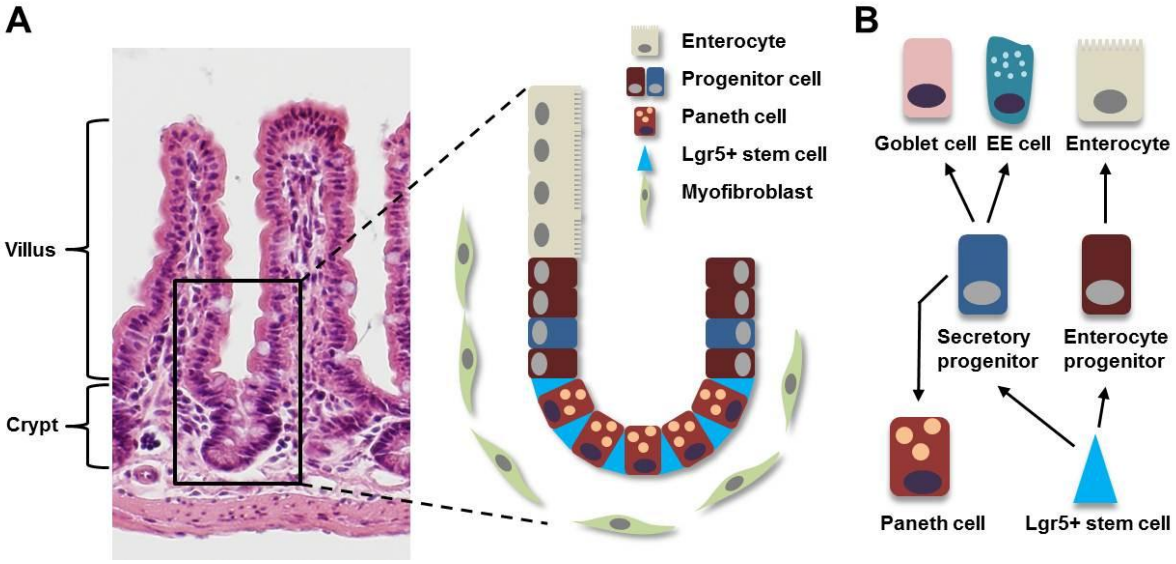
A
Villus
Crypt
Enterocyte
Progenitor cell
Paneth cell
Lgr5+ stem cell
Myofibroblast
B
Goblet cell
EE cell
Enterocyte
Secretory progenitor
Enterocyte progenitor
Paneth cell
Lgr5+ stem cell

Intestinal stem cells

Intestinal stem cells (ISCs) reside at the bottom of the crypt of Lieberkühn and fuel up the whole intestinal epithelium. These ISCs persist throughout the lifetime, and are capable of differentiating into any lineages of the intestinal epithelial cell.

Traditionally, an adult stem cell is described as a slow cycling, long-lived, multi-potent and asymmetrically dividing cell. The DNA labeling experiments showed that the cells at the +4 position within the intestinal crypt retain thymidine DNA labels long term. These +4 cells were assumed as ISCs. Later, studies showed that the +4 cells were proliferative and capable of self-renewal. Importantly the cells specifically express Bmi1, so Bmi1 expression has been widely considered as a marker of ISCs (Sangiorgi and Capecchi, 2008).

Using lineage tracing experiment, Barker et al also showed that crypt base columnar cell can generate all the intestinal epithelial cell lineages and serve as ISC in adult intestine (Barker et al., 2007). These CBC cells are relatively rapidly dividing, interspersed with Paneth cells and express R-spondin receptor, Lgr5. More recently, under specific condition, the $Lgr5^{+}$ cells are capable of forming intestinal epithelium-like structure *in vitro*, called the intestinal organoids (Sato et al., 2009). Differential gene expression analysis indicated that $Lgr5^{high}$ cells specifically express other marker genes including Olfm4 and Ascl2 (van der Flier and Clevers, 2009; van der Flier et al., 2009). Olfm4 is a glycoprotein that belongs to the olfactomedian protein family, promotes proliferation and cell adhesion. Ascl2 is a basic

helix loop helix transcription factor and positively regulates Wnt signaling cooperating with β-catenin.

It has been proposed that the ISCs can be sub-categorized into two distinct populations as described above: The $Bmi1^{+}$, slow-cycling, label-retaining +4 cells which are activated upon injury or irradiation and The $Lgr5^{+}$, fast-cycling, interspersed with Paneth cells, organoid forming CBCs which constantly divide into progeny at the crypt base. A recent paper from Hans Clever's laboratory, however, has disputed this. They conducted single transcript in situ hybridization and transcript profiling in FACS-sorted $Lgr5^{high}$ cells to show all of the markers of the +4 cells overlap and appear to be a gradient expression at the crypt base, not in specific position (Munoz et al., 2012).

More recently, This controversial idea that two distinct ISC populations exist in the crypt has been studied by Buczacki *et al*, who revealed that the label retaining +4 cells are in fact more committed population to the secretory lineage and differentiate into Paneth and enteroendocrine cells in homeostasis condition. However, after severe damage like irradiation, these relatively quiescent cells can rapidly proliferate and produce all of the epithelial lineages (Buczacki et al., 2013). Johan *et al*. also showed that $Dll1^{+}$ secretory lineage precursor can convert back to $Lgr5^{+}$ stem cell under irradiation (van Es et al., 2012). These influential studies suggest that the +4 cells which are previously considered as quiescent ISCs may be secretory progenitor population that rarely proliferates throughout lifetime.

All of the conflicting publication makes it very difficult to conclude the definition of ISCs. However, lots of the current literatures consider that fast-cycling $Lgr5^{+}$ stem cells are key stem cell population in intestinal crypt (Fig. 2).

The ISC niche is the microenvironment in which the ISCs reside. This niche provides a range of signal that supports ISC to be established and maintained. Paneth cells is major cellular component of the ISC niche because they express multiple signaling stimulus including EGF, Wnt3a and Dll4 which are necessary in both the establishment and maintenance of *in vitro* culture of ISCs (Sato et al., 2011; Sato et al., 2009). Because of the importance of Wnt signaling in the homeostasis of ISC population and the fact that the Paneth cells express Wnt3a ligands, the major role of the Paneth cells in ISC niche is the ability to supply Wnt ligands at the very adjacent from the ISC. However Kim *et al*. generated conditional *Atoh1*$^{-/-}$ mice and showed that the ISCs maintained normally in the absence of Paneth cells (Kim et al., 2012b). Also, recent genetic and chemical approaches suggest that there are abundant sources of Wnt ligands around the intestinal crypt including myofibroblast (San Roman et al., 2014). Despite the contradictory evidence, it is clear that the Paneth cells is important niche for the maintenance of the $Lgr5^{+}$ ISCs, however their exact role is still remains to be elucidated.

In 2009 Sato *et al.* published a remarkable method which enabled the growth of intimal epithelial structure *in vitro* called, intestinal organoids. These intestinal organoids

were grown from single intestinal crypts and consisted of multiple intestinal epithelium-like structures formed by crypt fission. The organoids can also be generated from single $Lgr5^+$ cells, thereby reinforcing the Lgr5 as a marker of the ISC population (Sato et al., 2009). The condition of intestinal organoid culture mimics those found within the intestinal crypt; the crypts or $Lgr5^+$ cells are cultured in Matrigel, which supports the cells to grow in 3-dimensional structure and also supply laminin-rich circumstances preventing anoikis. Epidermal growth factor is supplied in culture medium as it is known to support intestinal proliferation. BMP signaling pathway is inhibited by Noggin because BMP signaling is known to inhibit intestinal stem cell self-renewal (He et al., 2004). Importantly, R-spondin1 (Rspo1) is also obligatory for intestinal organoid culture. Rspo1 binds to its receptors, Lgr4 and Lgr5, which inhibit Rnf43/Znrf3 E3 ligases and finally activate Wnt/β-catenin signaling in ISCs. The intestinal organoid contains all the intestinal epithelial cell types found within the intestine and is structurally very similar to intestinal tissue.

This method is not only a highly beneficial tool to test drugs, but a handy way to understand the ISC biology. By altering the growth factor which enables crypts or $Lgr5^+$ cells to form organoids, it could be helpful to understand what factor is essential for an ISC to be as an ISC.

Figure 2. Intestinal stem cell and its plasticity (A) $Lgr5^+$ label-retaining cells are precursor of Paneth cell. Delta-like 1- expressing secretory progenitor cells supply goblet cells, endocrine cells and tuft cells. (B) Acute injury such as irradiation results in the loss of the proliferating $Lgr5^+$ stem cells, +4 stem cells and other cell populations can revert back to $Lgr5^+$ stem cells under loss of the $Lgr5^+$ stem cells.

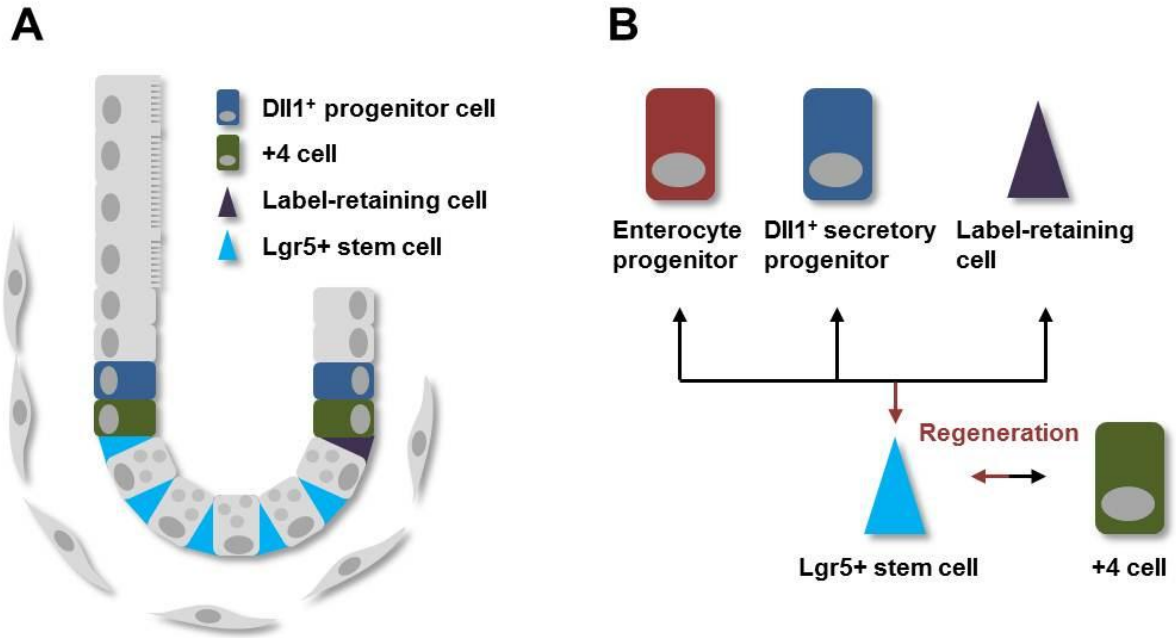
A
Dll1+ progenitor cell
+4 cell
Label-retaining cell
Lgr5+ stem cell
B
Enterocyte progenitor
Dll1+ secretory progenitor
Label-retaining cell
Regeneration
Lgr5+ stem cell
+4 cell

Signaling pathways regulating intestinal homeostasis - Wnt and Notch signaling

The delicate balance of cell proliferation, migration and apoptosis within the intestinal epithelium must be carefully organized in order to maintain intestinal structure and function. This balance can be achieved by controlling a number of important signaling pathways.

Canonical Wnt/β-catenin signaling is an essential signaling pathway in embryonic development because of its role in establishing the basic pattern of body (Fig. 3). The Wnt/β-catenin signaling pathway relies on the simple ligand-receptor binding. In the absence of Wnt ligands, the proteins in β-catenin degradation complex including Axin and adenomatous polyposis coli (APC) are phosphorylated by glycogen synthase kinase-3β (GSK3β) which increases their binding affinity to β-catenin. When β-catenin binds to these proteins GSK3β phosphorylates β-catenin, resulting in the proteasome dependent degradation of β-catenin. When Wnt ligands bind to its receptor, Frizzled and low density lipoprotein receptor-related protein (LRP), Dishevelleds (DVL) form a signaling platform and interact with AXIN, making it unavailable for binding to β-catenin and initiating its breakdown (Logan and Nusse, 2004). The 'free' β-catenin accumulates and translocate to the nucleus, where it cooperates with lymphoid enhancer-binding factor 1 and T cell-specific transcription factor (LEF/TCF) to induce transcription of Wnt/β-catenin target genes (Clevers, 2006).

The Wnt/β-catenin signaling mainly associated with cellular process including

proliferation, migration and adhesion which are required for ISC maintenance. Indeed, the appropriate regulation of Wnt/β-catenin signaling is pivotal for the maintenance of the ISC population. In the absence of Wnt receptor or presence of Wnt antagonist, the ISC loose its activity and eventually the intestinal crypt degenerated (Pinto et al., 2003). The importance of Wnt/β-catenin signaling within intestinal homeostasis has been also demonstrated using other experimental formats. Ireland *et al.* showed that conditional deletion of β-catenin in intestinal epithelium of mice resulted in deleterious disruption of intestinal epithelium with crypt ablations (Ireland et al., 2004).

Notch signaling is juxtacrine signaling pathway, meaning that the signaling can only be activated via direct cell-to-cell contact with adjacent cells (Fig. 4). Notch ligands such as Jagged or Delta bind with the Notch receptor and cause proteolytic cleavage events. The tumor necrosis factor-α-converting enzyme (TACE), mediate the first cleavage of the extracellular domain of Notch receptor. When the first clevage has occurred, the second cleavage takes place by γ-secretase, releasing the Notch intracellular domain (NICD) into cytosol. The released NICD translocates into the nucleus and cooperate with the transcription factor CSL to express various Notch target genes. The Notch target genes have various functions which influence tissue homeostasis via controlling apoptosis, proliferation, patterning and fate determination of cells (Artavanis-Tsakonas et al., 1999). Although chemical inactivation of Notch signaling bt γ-secretase inhibitor induces conversion of

proliferative progenitors in the intestinal epithelium into secretory goblet-like cells (van Es et al., 2005), the role of Notch signaling in ISC remain unclear. The importance of Notch signaling in ISC is, however, reinforced by the expression of Notch ligands and the presence of NICD found at the base of the crypt compared to the rest of the epithelium.

Figure 3. The Wnt signaling pathway. When Wnt ligands bind to its receptor, Dishevelleds (Dvl) form a signaling platform and interact with AXIN, resulting in dissociation of degradation complex of β-catenin. β-catenin subsequently accumulates and translocates to the nucleus, forming a complex with T cell-specific transcription factor/lymphoid enhancer-binding factor family to control target gene expressions

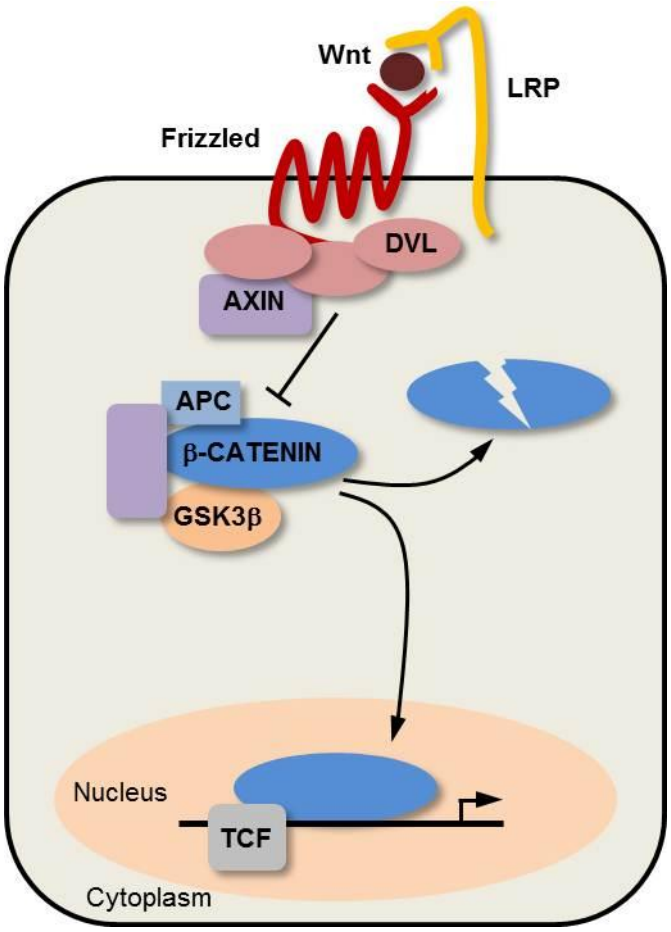
Wnt
LRP
Frizzled
DVL
AXIN
APC
β-CATENIN
GSK3β
Nucleus
TCF
Cytoplasm

Figure 4. The Notch signaling pathway. When Notch receptors bind to ligand presented by signal-sending cells, S2 cleavage releases the extracellular domain of the Notch receptor, which induces endocytosis of the ligand by the signal-sending cell. Then, S3 cleavage can occur and release the Notch intercellular domain (NICD), which translocates into the nucleus, where it activates transcription. In the nucleus, NICD recruits coactivators such as Mastermind-like 1 (MAML) and Recombining binding protein suppressor of hairless (RBPJ).

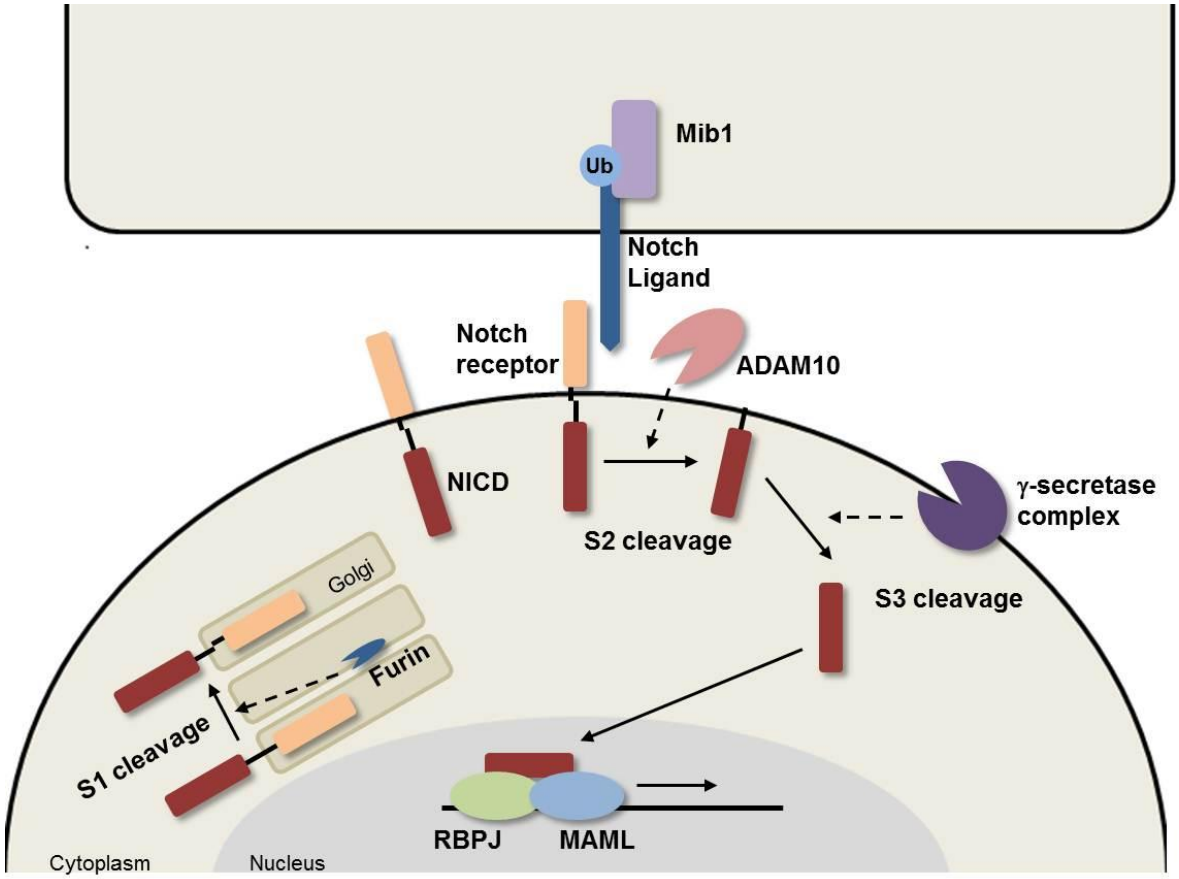
Mib1
Ub
Notch
Ligand
Notch
receptor
ADAM10
NICD
S2 cleavage
γ-secretase
complex
S3 cleavage
Golgi
Furin
S1 cleavage
RBPJ
MAML
Cytoplasm
Nucleus

Intestinal tumorigenesis

Colorectal cancer (CRC) is the third most common cancer world-wide, with almost 1 million people being diagnosed every year. Even though its survival rates have been increased in the last 30 years, over half of patients cannot survive for longer than 5 years after first diagnosis. The intrinsic characteristic of intestinal epithelial cells associate with a high incidence of cancer. The high rate of cell division in the crypt results in a high frequency of DNA replication errors and so pile up the DNA mutations in proliferative cells such as ISCs. Also, the direct exposure to ingested food and potential carcinogens further increases the oncogenic mutation rate.

The development of sporadic colorectal cancer is a process with multiple steps wherein an accumulation of genetic mutations induces malignant progression of normal intestinal epithelium to metastatic carcinoma. Based on studies of gene alteration in human CRCs, Fearon and Vogelstein proposed that deleterious mutation in *Adenomatous polyposis coli (*APC) initiates the formation of a benign hyperplasia and other oncogenic mutations in KRAS and p53 contribute to the progression to malignant disease (Fearon and Vogelstein, 1990).

Since Wnt/β-catenin signaling has been reported to control a number of regulatory processes related with tumorigenesis, such as cell proliferation and adhesion, it is not surprising that defects within this pathway are oncogenic, particularly in CRC. Loss of APC

leads to defective degradation of β-catenin and results in accumulation of nuclear β-catenin, where it can cooperate with TCF as a transcription factor. *APC* was originally identified as the gene mutated in cases of familial adenomatous polyposis (FAP). FAP is an inherited autosomal disorder; patients develop multiple colonic adenomas at a young age. Although the polyps are relatively benign, there is a high risk that some can develop into malignant adenocarcinomas if left untreated (Groden et al., 1991).

In 1990 a genetic mouse model termed the Multiple Intestinal Neoplasia mouse (MIN), which modeled FAP, was identified in random mutagenesis study (Fig. 5). The mice carry a mutation that induces truncation of the protein at codon 850 in one allele of the mouse homologue of *APC* and develop multiple polyps throughout the entire intestinal tract from an early age (Moser et al., 1990). The development of the $Apc^{Min/+}$ model was a breakthrough in the study of CRC, and it leads to development of a variety of different *Apc* mutants. (Fodde et al., 1994). These *Apc* mutants provide exceptionally useful system to study the modulators in Wnt-dependent tumorigenesis. Using these mice, it was possible to dissect the regulatory pathway of intestinal tumorigenesis at various stages of tumor development.

Barker *et al.* showed that when *Apc* deletion occurred specifically in the $Lgr5^{+}$ ISC population, the ISC became microadenoma within 3-5 weeks and develop rapidly into adenomas, whereas when *Apc* is deleted specifically from intestinal progenitor population, microadenomas was not developed (Barker et al., 2009). The differentiated cells in intestinal

epithelium become rapidly shattered off at the tip of villi. Thus the loss of *Apc* in these cells also might have no effect. These results clearly show the critical link between the ISCs and tumorigenesis, and the expansion of the ISC compartment would provide the intestinal epithelium with a higher cancer risk.

Figure 5. APC^{Min} mouse model (A) *Apc^{Min}* allele carries a nonsense mutation in codon 850 of the *Apc* gene, leading to a truncated APC protein. Heterozygous *Apc$^{Min/+}$* (Min) animals develop more than 50 intestinal tumours per animal, mainly located in the small intestine. (B) When two alleles of APC are mutated, the degradation of β-catenin is inhibited. Subsequently, β-catenin accumulates and induces target gene expression.

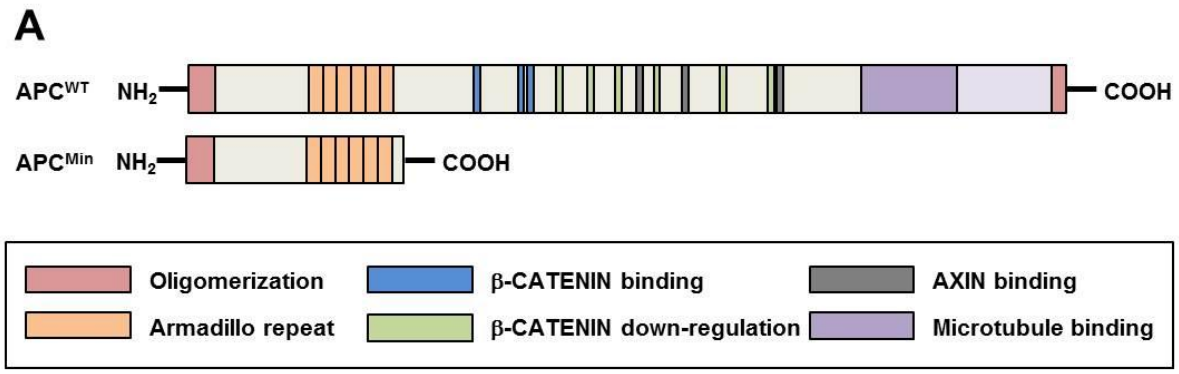
A
APC^WT
NH2
COOH
APC^Min
NH2
COOH
Oligomerization
Armadillo repeat
β-CATENIN binding
β-CATENIN down-regulation
AXIN binding
Microtubule binding

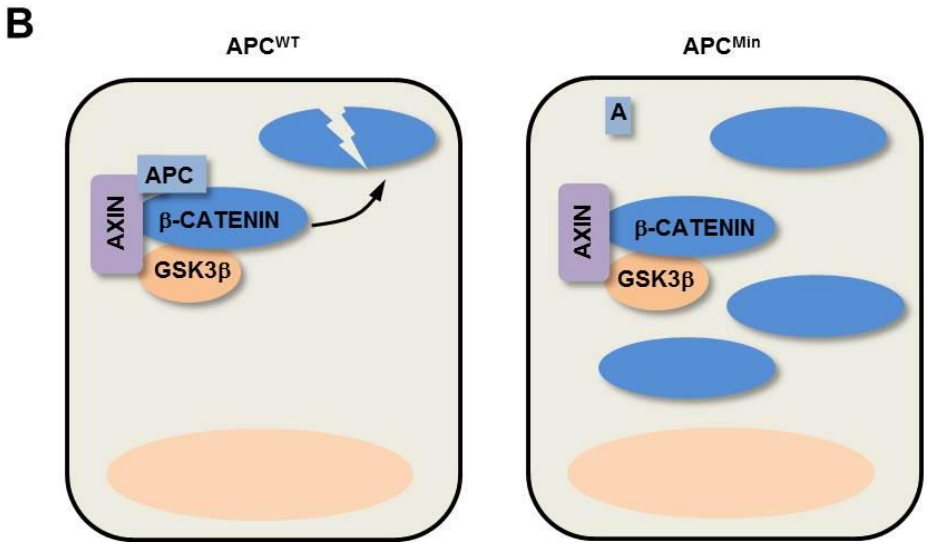
B
APC^WT
APC^Min
APC
AXIN
β-CATENIN
GSK3β
A
AXIN
β-CATENIN
GSK3β

Aminoacyl tRNA synthetase interacting multifunctional protein 2

Aminoacyl-tRNA synthetases (ARSs) are highly conserved enzymes that ligate the specific amino acids to cognate tRNAs in translation (Fig. 6A). These ARSs plays pivotal role that transfer right amino acids to protein synthesis machineries. Three non-enzymatic factors, aminoacyltRNA synthetase-interacting multi-functional protein (AIMP) 1, 2 and 3, form macromolecular complexes called multi-tRNA synthetase complex (MSC) with nine different ARSs. These AIMPs function as a scaffolding component of MSC that binds with ARSs for efficient translation (Park et al., 2005b). Although their canonical function is protein synthesis as housekeepers, many studies report their non-canonical functions especially in cancer cells. Recent analytical study revealed the differential expression of ARSs in malignant tissues and showed that ARSs interacts with cancer-associated proteins physically or genetically (Kim et al., 2011).

Aminoacyl-tRNA synthetase-interacting multi-functional protein2 (AIMP2) is one of the major scaffolding protein that stabilize the MSC for translation (Fig. 6B). Besides amino-acylation, AIMP2 is involved in other signaling pathways. Genetic disruption of *Aimp2* results in neonatal lethality by defects in lung differentiation. Upon binding of TGF-β, AIMP2 induces the degradation of Fuse binding protein and inhibits the transcription of *c-myc* (Kim et al., 2003). It has also been reported that AIMP2 induces apoptosis by promoting the degradation of TNF-receptor associated factor 2 (TRAF2) in the presence of TNF-α

ligand and the stabilization of p53 in response to DNA damage (Choi et al., 2009a; Han et al., 2008). These reports suggest that AIMP2 has anti-proliferative function and potentially act as a tumorsuppressor.

On the other hand, AIMP2 is a strong candidate as a pathogenic parkin substrate that accumulates in Parkinson's disease because of parkin inactivation (Ko et al., 2010; Ko et al., 2005). Interestingly, AIMP2 is increased in the ventral midbrain of *Parkin*$^{-/-}$ mice and post-mortem brain from patients with Parkinson's disease. Recently, Lee *et al.* showed that the overexpression of AIMP2 at the comparable level with Parkinson's disease leads to a severe degeneration of dopaminergic neurons that causes motor impairment (Lee et al., 2013).

Figure 6. Aminoacyl-tRNA synthetase and AIMP2. (A) Catalysis of Aminoacyl-tRNA synthetases. The enzymes consume ATP and generate Aminoacyl-tRNA. Because misrecognition of amino acids and its cognate tRNAs will result in the wrong polypeptides, They are highly specific in substrate recognition. (B) Cartoon represents a macromolecular Aminoacyl-tRNA synthetases complex, containing nine ARSs and three AIMPs. Each AIMP appear to interact with specific ARSs (solid lines).

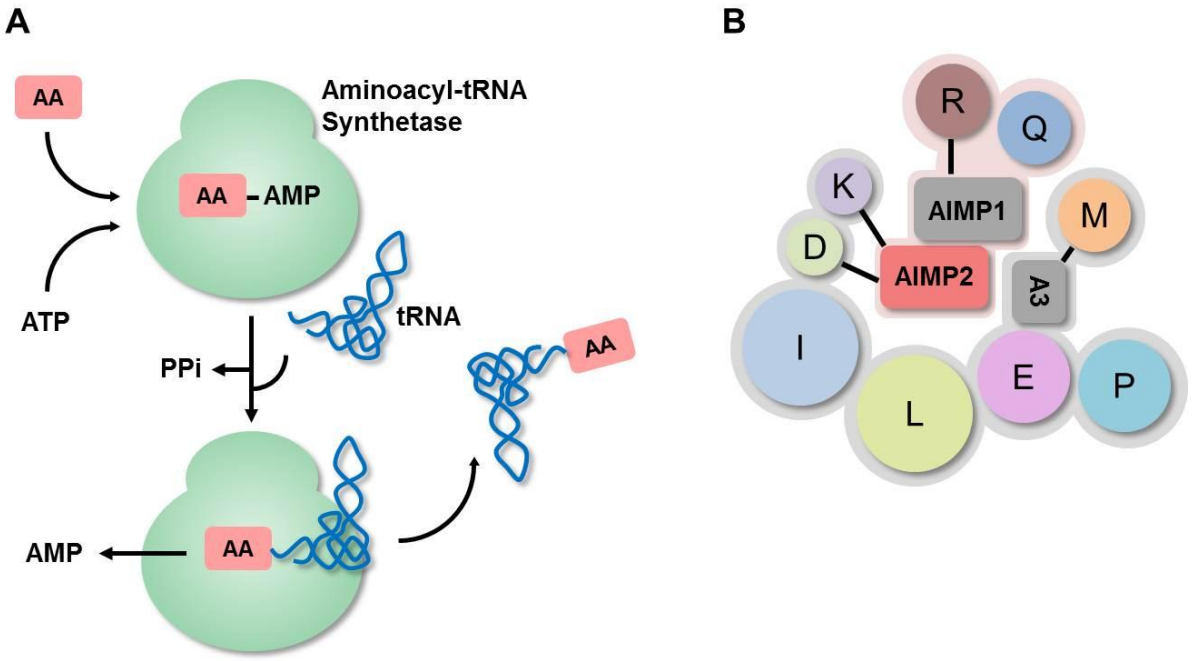
A
AA
Aminoacyl-tRNA
Synthetase
AA
AMP
ATP
tRNA
PPi
AA
AMP
AA
B
R
Q
K
AIMP1
M
D
AIMP2
A3
I
E
P
L

INTRODUCTION

The intestinal epithelium self-renews every three to five days through its highly proliferative compartment, the crypt of Lieberkühn. Intestinal stem cells (ISCs) expressing leucine rich repeat-containing G-protein coupled receptor 5 (LGR5) residing at the bottom of crypts generate all types of cells in the intestinal epithelium (Barker et al., 2007). Cryptal mesenchymal cells and Paneth cells (PCs) constitute the ISC niche and support the maintenance of ISCs by producing factors such as epidermal growth factor, Notch, and Wnt (Sato et al., 2011).

Wnt/β-catenin signaling plays a pivotal role in homeostatic self-renewal of ISCs (Clevers and Nusse, 2012). Binding of Wnt ligands to its receptors, Frizzled and low density lipoprotein receptor-related protein 5/6 (LRP5/6) activate a signaling cascade inhibiting the β-catenin destruction complex, which contains axis inhibition protein (AXIN), adenomatous polyposis coli (APC), and glycogen synthetase kinase 3β (GSK3β). β-catenin subsequently accumulates and translocates to the nucleus, forming a complex with T cell-specific transcription factor/lymphoid enhancer-binding factor family to control target gene expressions (Cadigan and Peifer, 2009), which supports the maintenance, proliferation, and differentiation of ISCs.

Disruption of Wnt/β-catenin signaling leads to ISC depletion and crypt degeneration

(Korinek et al., 1998; Pinto et al., 2003). Conversely, constitutive activation of Wnt/β-catenin signaling in the intestinal epithelium drives excessive cell proliferation and tumor formation (van de Wetering et al., 2002). Approximately 80% of human sporadic colorectal tumors are caused by mutations in the *APC* gene, and mice lacking the *Apc* gene in ISCs develop severe polyposis (Barker et al., 2009). These studies suggest that the activity of Wnt/β-catenin signaling should be tightly regulated, albeit ISCs require Wnt/β-catenin signaling to maintain their stemness. Interestingly, despite abundant sources of Wnt ligands at the crypt base (Farin et al., 2012), Wnt/β-catenin signaling is not fully activated in ISCs. Recently, Koo et al. reported that the RNF43 and ZNRF3 E3 ligases ubiquitinate Wnt receptors and inhibit Wnt/β-catenin signaling (Koo et al., 2012). Importantly, *Rnf43*/*Znrf3* compound mutant mice show increased intestinal proliferation and eventually develop adenomas that phenocopy the *Apc* mutant mice (Barker et al., 2009), suggesting that inhibition of Wnt/β-catenin signaling by RNF43 and ZNRF3 is critical for suppressing ISC proliferation. Nevertheless, *Rnf43/Znrf3* mutant adenomas showed low-grade characteristics, including smaller adenoma size and less abrogated epithelial structure when compared with *Apc* mutant mice. These differences suggest that additional regulatory mechanisms exist between the Wnt receptor and the β-catenin destruction complex.

The aminoacyl-tRNA synthetases (ARSs) are catalytic enzymes that attach specific amino acids to their corresponding tRNAs. Nine different ARSs form the multi-tRNA

synthetase complex associating with three non-enzymatic ARS-interacting multifunctional proteins (AIMPs), AIMP1, AIMP2 and AIMP3, which stabilize the assembly of ARSs into the multi-tRNA synthetase complex (Quevillon et al., 1999). Despite "housekeeping" functions of ARSs and AIMPs in protein synthesis, accumulating evidence indicates they have noncanonical functions beyond protein synthesis (Kim et al., 2011). For instance, after genotoxic stress, AIMP3 translocates to the nucleus activating p53 through the activation of the kinases ataxia telangiectasia mutated (ATM) and ATM- and Rad3-related (ATR) (Park et al., 2005a). Some ARSs and AIMPs, such as tyrosyl-tRNA synthetase and AIMP1, are secreted as extracellular signaling factors controlling angiogenesis and immune responses (Ko et al., 2001; Wakasugi et al., 2002). AIMP2 is also involved in other signaling pathways besides amino-acylation. Genetic disruption of *Aimp2* results in neonatal lethality by defects in lung differentiation (Kim et al., 2003). It has also been reported that AIMP2 induces apoptosis by promoting the degradation of TNF-receptor associated factor 2 (TRAF2) and the activation of p53 in response to DNA damage (Choi et al., 2009a; Han et al., 2008). Interestingly, the activity of AIMP2 seems highly sensitive to *Aimp2* gene dosage, suggesting that the level of AIMP2 is important for its roles as a signaling modulator (Choi et al., 2009b).

Here, I investigated the effect of AIMP2 haploinsufficiency in the intestinal epithelium and tumorigenesis using mouse models and an organoid culture system. I found that hemizygous deletion of the *Aimp2* gene enhanced the initiation of intestinal adenoma

formation in *Apc*$^{Min/+}$ mice. AIMP2 was highly expressed in the crypt compared to the villus, and hemizygous deletion of *Aimp2* led to the expansion of ISCs and PCs, which constitute the ISC compartment. Consistently, the expression of Wnt target genes were markedly increased in *Aimp2*$^{+/-}$ intestines compared to *Aimp2*$^{+/+}$. At the mechanistic level, AIMP2 bound to Dishevelled (DVL) and disrupted DVL-AXIN interaction, thereby inhibiting Wnt/β-catenin signaling. Importantly, *in vitro* and organoid formation analyses using *Aimp2*$^{+/+}$, *Aimp2*$^{+/-}$, and *Aimp2*$^{-/-}$ mouse embryonic fibroblasts (MEFs) and intestinal epithelial cells (IECs) showed that the activity of Wnt/β-catenin signaling negatively correlated with AIMP2 dosage. Collectively, our results reveal a pivotal role for AIMP2 in fine-tuning of Wnt/β-catenin signaling activity in the intestinal epithelium.

RESULT

Hemizygous deletion of *Aimp2* in *Apc*$^{Min/+}$ mice results in enhanced tumor burden

To investigate whether AIMP2 haploinsufficiency affects intestinal tumorigenesis, I crossed *Aimp2*$^{+/-}$ mice with *Apc*$^{Min/+}$ mice (Moser et al., 1990). Interestingly, *Aimp2*$^{+/-}$:*Apc*$^{Min/+}$ mice exhibited significantly reduced survival rates when compared with *Aimp2*$^{+/+}$:*Apc*$^{Min/+}$ mice (Fig. 7).

Consistently, methylene blue staining of whole intestinal tracts showed that the number of polyps significantly increased in both genders of 20-week-old *Aimp2*$^{+/-}$:*Apc*$^{Min/+}$ mice (average 98.4 polyps per mouse) than in *Aimp2*$^{+/+}$:*Apc*$^{Min/+}$ littermates (average 62.4 polyps per mouse) (Fig. 8*A*). Polyp counting on intestinal segments including Duodenum, Jejunum, Ileum and Colon showed general increase of polyp formation in *Aimp2*$^{+/-}$:*Apc*$^{Min/+}$ intestine (Fig. 8*B*). The polyps in *Aimp2*$^{+/-}$:*Apc*$^{Min/+}$ mice were notably larger than those in *Aimp2*$^{+/+}$:*Apc*$^{Min/+}$ mice (Fig. 8*C*). Remarkably, about 50% of the polyps in *Aimp2*$^{+/-}$:*Apc*$^{Min/+}$ mice had a diameter larger than 2 mm, compared with 24% of the polyps in *Aimp2*$^{+/+}$:*Apc*$^{Min/+}$ mice (Fig. 8*D*). Although the size of the polyps increased in *Aimp2*$^{+/-}$:*Apc*$^{Min/+}$ mice, invading tumors were not detected, even in moribund *Aimp2*$^{+/-}$:*Apc*$^{Min/+}$ mice (data not shown).

To investigate whether the increase in polyp number and size in *Aimp2*$^{+/-}$:*Apc*$^{Min/+}$ mice were due to earlier tumor initiation, I examined tumor initiation by counting aberrant crypt foci (ACF), the preneoplastic lesions of intestinal tumors (Takayama et al., 1998). Histological analysis of the whole small intestine from 6-week-old mice showed that the number of ACF increased in *Aimp2*$^{+/-}$:*Apc*$^{Min/+}$ mice (average 18.9 ± 3.1 per section) than that in *Aimp2*$^{+/+}$:*Apc*$^{Min/+}$ mice (average 11.5 ± 3.6 per section) (Fig. 9*A*). Consistently, large tumors were readily observed in 7-week-old *Aimp2*$^{+/-}$:*Apc*$^{Min/+}$ mice, but not in the littermate controls (Fig. 9*B*), indicating that *Aimp2*$^{+/-}$:*Apc*$^{Min/+}$ mice had accelerated tumor formation. Collectively, these results suggest that AIMP2 acts as a haploinsufficient tumor suppressor in intestinal tumorigenesis.

Figure 7. Hemizygous deletion of *Aimp2* decreases survival of $Apc^{Min/+}$ mice. (A) Kaplan-Meier Survival graph of $Aimp2^{+/+}$:$Apc^{Min/+}$ (n = 24) and $Aimp2^{+/-}$:$Apc^{Min/+}$ (n = 17) littermates. The *P*-value is based on the log-rank test.

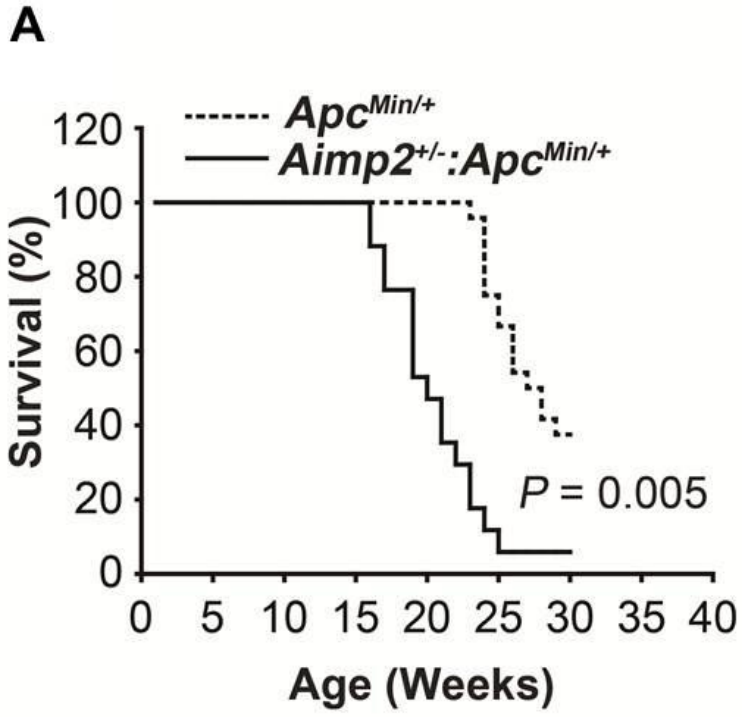
A
Apc^Min/+
Aimp2^+/-:Apc^Min/+
Survival (%)
120
100
80
60
40
20
0
P = 0.005
0 5 10 15 20 25 30 35 40
Age (Weeks)

Figure 8. Tumor burden is increased in *Aimp2*$^{+/-}$:*Apc*$^{Min/+}$mice (A-B) Polyp numbers in 20-week-old *Aimp2*$^{+/+}$:*Apc*$^{Min/+}$ (n = 23) and *Aimp2*$^{+/-}$:*Apc*$^{Min/+}$ (n = 24) whole intestines (A) and different intestinal segments (B, Duo: duodenum, Jej: jejunum, Ile: ileum, and Col: colon). (C) Methylene blue staining of the ileums. The polyps are circled with white dashed lines. (D) Size distribution of polyps in *Aimp2*$^{+/+}$:*Apc*$^{Min/+}$ (n = 6) and *Aimp2*$^{+/-}$:*Apc*$^{Min/+}$ (n = 4) intestine. Data are the mean ± standard error of the mean (SEM). *$P < 0.01$.

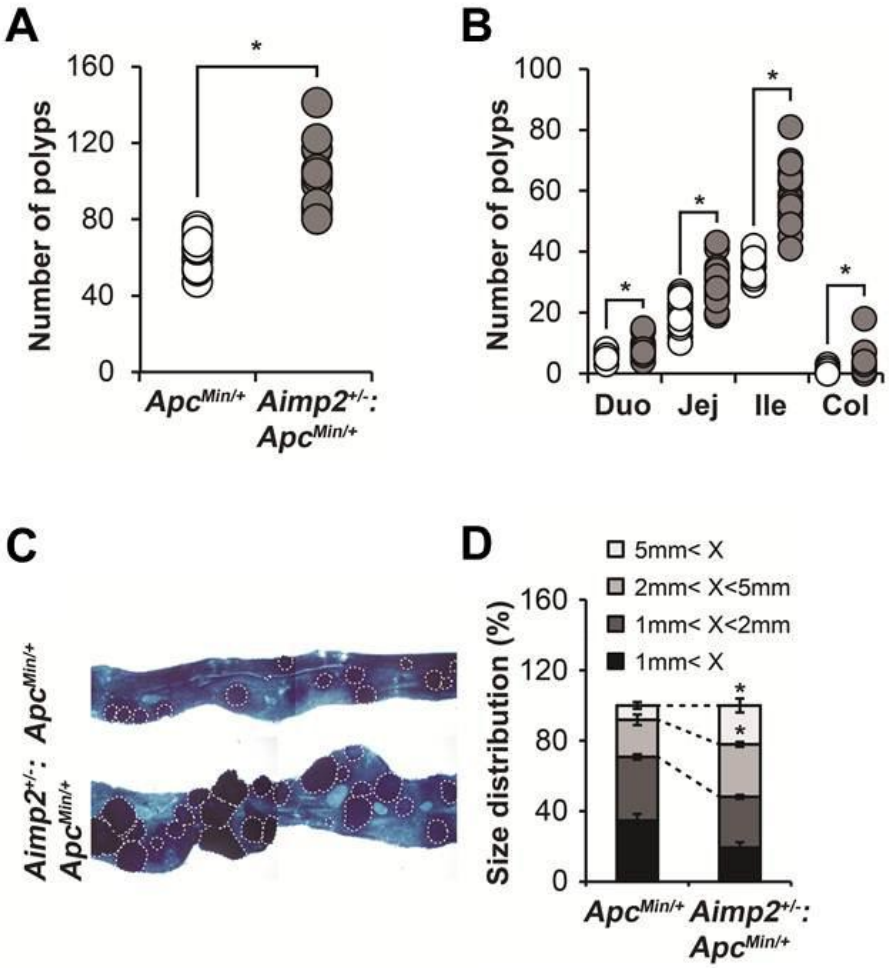
A
Number of polyps
160
120
80
40
0
*
ApcMin/+
Aimp2+/-:
ApcMin/+
B
Number of polyps
100
80
60
40
20
0
*
Duo
Jej
Ile
Col
C
Aimp2+/-: ApcMin/+
ApcMin/+
D
5mm< X
2mm< X<5mm
1mm< X<2mm
1mm< X
Size distribution (%)
160
120
80
40
0
ApcMin/+
Aimp2+/-:
ApcMin/+

Figure 9. Tumor initiation is increased in *Aimp2*$^{+/-}$:*Apc*$^{Min/+}$ mice (A) Numbers of ACF in 6-week-old *Aimp2*$^{+/+}$:*Apc*$^{Min/+}$ (n = 5) and *Aimp2*$^{+/-}$:*Apc*$^{Min/+}$ (n = 5) intestine. One of every five consecutive sections was examined. ACF were quantified in 10 sections. (B) H&E staining of small intestines from 7-week-old mice. Polyps are circled with black dashed lines. Student *t*-test was applied, and data are the mean ± standard error of the mean (SEM). *$P < 0.01$.

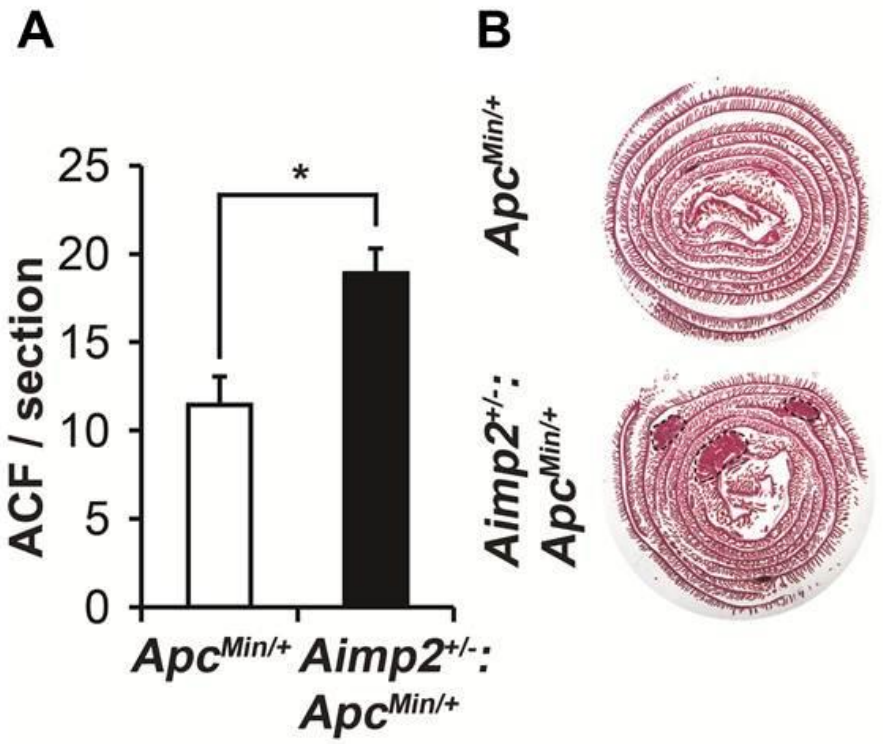
A
B
ACF / section
25
20
15
10
5
0
*
Apc^Min/+
Aimp2^+/-:
Apc^Min/+
Apc^Min/+
Aimp2^+/-:
Apc^Min/+

Hemizygous deletion of *Aimp2* increases proliferation in the crypts

To investigate a role of AIMP2 in IECs, I examined the expression pattern of AIMP2 in intestine. At embryonic day 18.5, AIMP2 was highly expressed at the intervillus region of *Aimp2*$^{+/+}$ intestine but not in *Aimp2*$^{-/-}$ (Fig. 10*A*), indicating that the antibody is specific to AIMP2. In the adult intestine, AIMP2 was highly expressed in the crypt, where it predominantly localized in the cytosol (Fig. 10*B*). Consistent with immunohistochemical detection of AIMP2 in crypt, *Aimp2* mRNA expression in the crypt fractions was about 2.5-fold higher than that in the villus fractions (Fig. 10*C*), suggesting that AIMP2 functions in the crypts.

Because loss of heterozygosity (LOH) in *Apc*$^{Min/+}$ mice is a stochastic event (Haigis et al., 2002), intestinal tumor formation in *Apc*$^{Min/+}$ mice depends on the proliferation rate of IECs, including ISCs in which LOH should occur (Barker et al., 2009). Therefore, I examined whether hemizygous deletion of *Aimp2* affected the proliferation of IECs, including ISCs. The lengths of the crypt and villus were increased in heterozygous *Aimp2*$^{+/-}$ mice compared to *Aimp2*$^{+/+}$ (Fig. 11A-C). The number of Ki67^{+} cells increased in the *Aimp2*$^{+/-}$ crypts (*Aimp2*$^{+/+}$: 17.8 ± 4.7 vs. *Aimp2*$^{+/-}$: 27.4 ± 4.9 per crypt) (Fig. 12*A* and *B*). To confirm these results, I injected mice with bromodeoxyuridine (BrdU) 2 hr before sacrifice and counted BrdU-labeled cycling cells. As expected, the number of BrdU^{+} cells significantly

increased in the *Aimp2*$^{+/-}$ crypts (*Aimp2*$^{+/+}$: 12.3 ± 3.1 vs. *Aimp2*$^{+/-}$: 19.5 ± 4.4 per crypt) (Fig. 12*C* and *D*).

Notably, AIMP2 is also highly expressed in the bottom of the colonic crypts (Fig. 13*A*). The number of Ki67^{+} cells was also increased in the *Aimp2*$^{+/-}$ colon (*Aimp2*$^{+/+}$: 10.7 ± 1.9 vs. *Aimp2*$^{+/-}$: 17.7 ± 3.2 per crypt) (Fig. 13*B* and *C*). TUNEL and cleaved caspase-3 staining revealed that apoptosis of IECs is not affected when AIMP2 is reduced (Fig. 14*A*-*D*). Taken together, these results suggest that AIMP2 inhibits the proliferation of IECs in the crypts throughout the intestine.

Figure 10. AIMP2 is highly expressed in intestinal crypt (A-B) Immunohistochemical staining of AIMP2 in E18.5 (A) and 20-week-old (B) intestine. (C) mRNA expressions in villi/crypt fractions from wild-type mice (n = 3). Scale bar, 50 μm. Student *t*-test was performed, and data are the mean ± SEM. *$P < 0.01$.

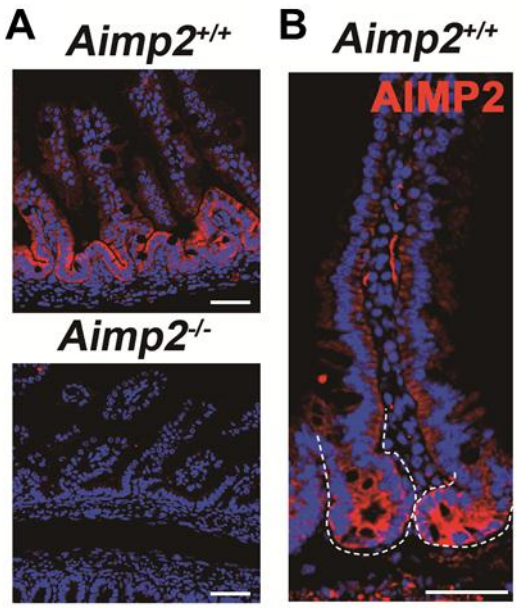
A
Aimp2+/+
Aimp2-/-
B
Aimp2+/+
AIMP2

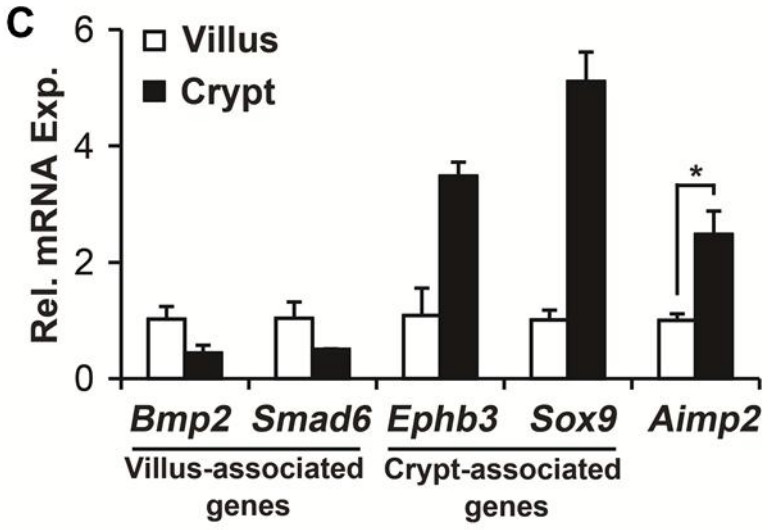
C
Rel. mRNA Exp.
6
4
2
0
Villus
Crypt
*
Bmp2
Smad6
Ephb3
Sox9
Aimp2
Villus-associated genes
Crypt-associated genes

Figure 11. *Aimp2*$^{+/-}$ mice exhibit increased villi length and crypt depth (A) Representative H&E staining in ileums of 20-week-old *Aimp2*$^{+/+}$ and *Aimp2*$^{+/-}$. (B-C) Quantification of villi length (B) and crypt depth (C) in *Aimp2*$^{+/+}$ (n = 3) and *Aimp2*$^{+/-}$ littermates (n = 3). Graph presents the villi length and crypt depth in different regions of the intestine (Duo: duodenum, Jej: jejunum, and Ile: ileum). Scale bar, 50 μm. Student *t*-test was performed, and data were presented as the mean ± standard error of the mean. *$P < 0.01$.

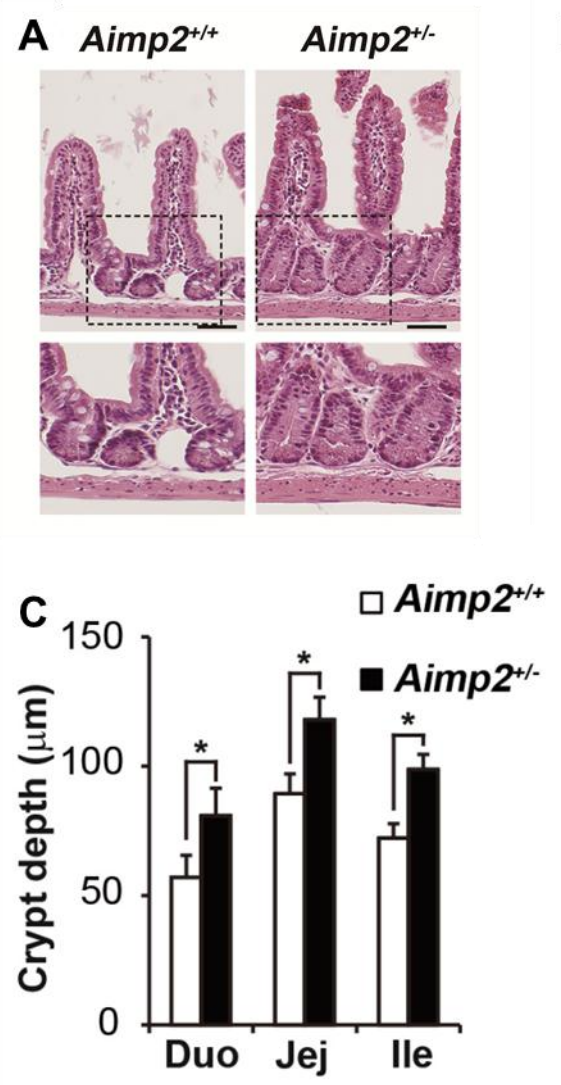
A
Aimp2+/+
Aimp2+/-
B
Aimp2+/+
Aimp2+/-
Vili length (μm)
600
400
200
0
Duo
Jej
Ile
C
Aimp2+/+
Aimp2+/-
Crypt depth (μm)
150
100
50
0
Duo
Jej
Ile

Figure 12. AIMP2 inhibits epithelial cell proliferation in the intestinal crypt (A-D) Immunohistochemical staining and quantification of Ki67 (A, B) and BrdU (C, D) in ileal crypts of 20-week-old *Aimp2*$^{+/+}$ (n = 3) and *Aimp2*$^{+/-}$ (n = 3). White arrows indicate Ki67^{+} or BrdU^{+} crypt base cells respectively. The crypts are outlined by white dashed lines (E,G). At least 30 well-oriented crypts were analyzed on 3-4 slides per mouse. Scale bar, 50 μm. Student *t*-test was performed, and data are the mean ± SEM. *$P < 0.01$.

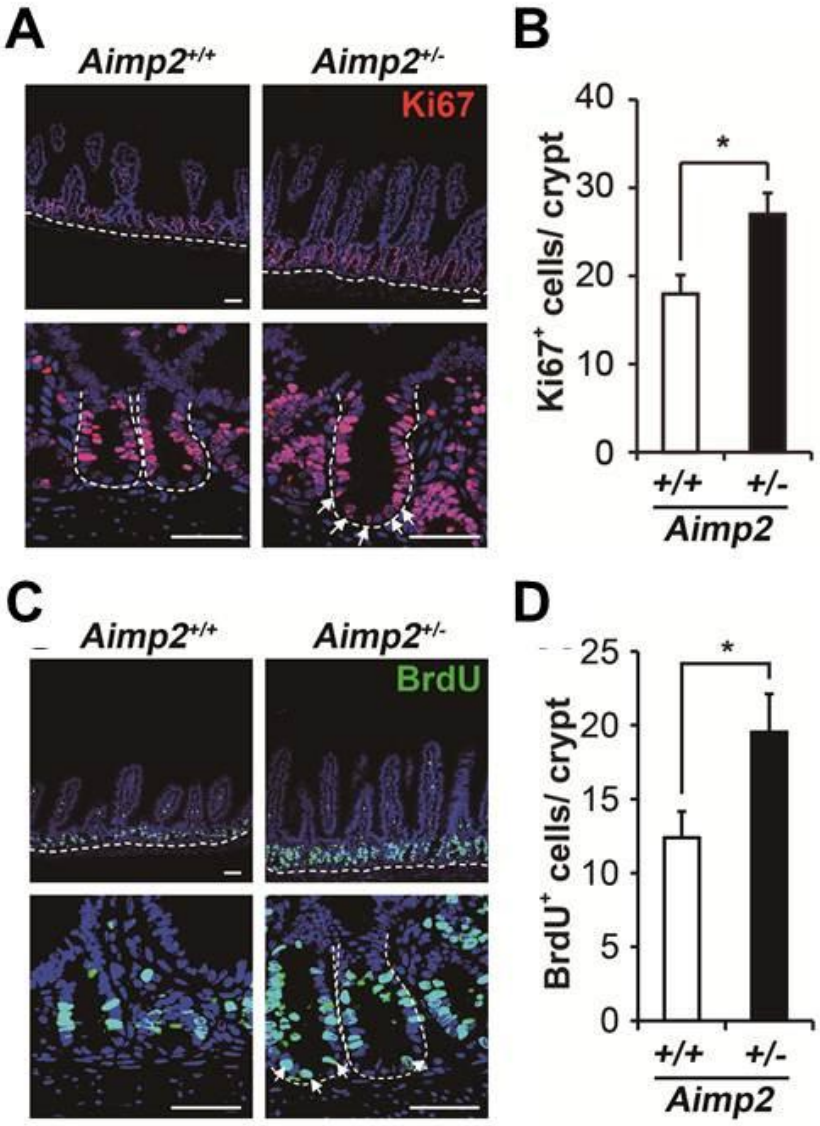
A
Aimp2+/+
Aimp2+/-
Ki67
B
Ki67+ cells/ crypt
40
30
20
10
0
*
+/+
+/-
Aimp2
C
Aimp2+/+
Aimp2+/-
BrdU
D
BrdU+ cells/ crypt
25
20
15
10
5
0
*
+/+
+/-
Aimp2

Figure 13. AIMP2 also inhibits proliferation of the colonic epithelial cells (A) Immunohistochemistry with AIMP2 antibody on sections of the adult (20-week-old) colon. (B) Representative images of Ki67 immunohistochemistry in the colonic crypts of 20-week-old *Aimp2*$^{+/+}$ and *Aimp2*$^{+/-}$ littermates. (C) Quantification of Ki67^{+} cells in *Aimp2*$^{+/+}$ (n = 5) and *Aimp2*$^{+/-}$ (n = 5) colonic crypts. At least 30 well-oriented crypts were analyzed on 3–4 slides for each mouse. Student *t*-test was performed, and data were presented as the mean ± standard error of the mean. **P* < 0.01.

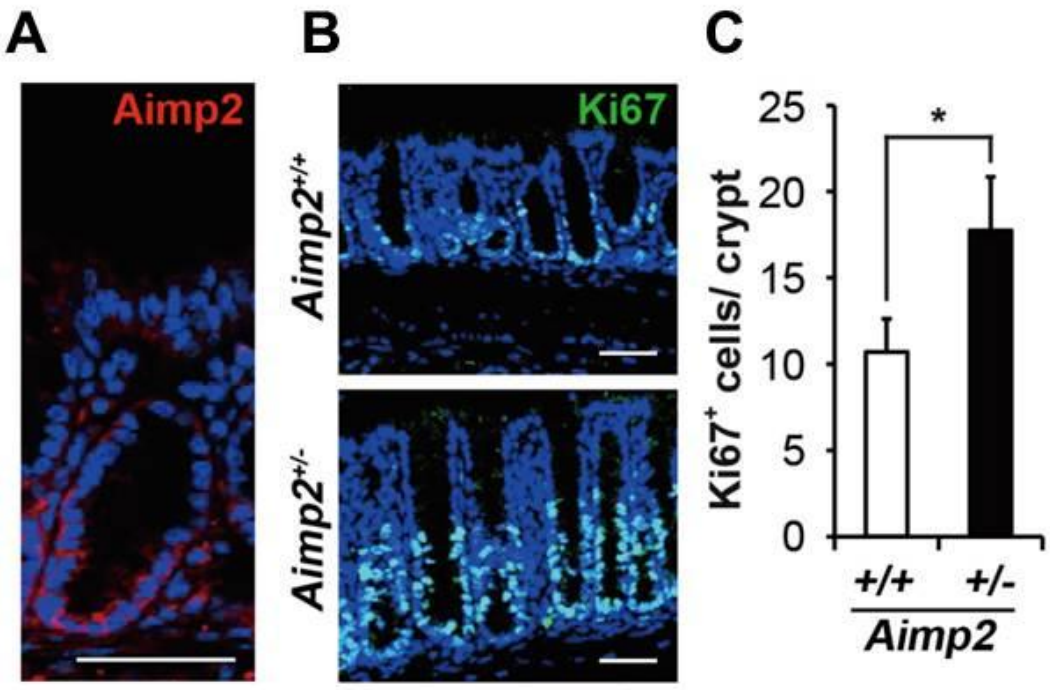
A
Aimp2
B
Ki67
Aimp2+/+
Aimp2+/-
C
25
20
15
10
5
0
*
Ki67+ cells/ crypt
+/+
+/-
Aimp2

Figure 14. AIMP2 does not affect the apoptosis of intestinal epithelial cells (A-B) Immunohistochemical staining (A), and quantification (B) of cleaved-Caspase3 in 20-week-old *Aimp2*$^{+/+}$ (n = 5) and *Aimp2*$^{+/-}$ villi (n = 5). White arrows indicate cleaved-Caspase3^{+} cells in the villus. At least 30 well-oriented villi were analyzed on 3-4 slides per mouse. (C) Representative images of TUNEL staining in intestinal sections (ileum) from 6-week-old *Aimp2*$^{+/+}$ and *Aimp2*$^{+/-}$ littermates. (D) Quantification of TUNEL^{+} cells in *Aimp2*$^{+/+}$ (n = 5) and *Aimp2*$^{+/-}$ villi (n = 5). Scale bar, 50 μm. Student *t*-test was performed, and data are the mean ± SEM. **P* < 0.01.

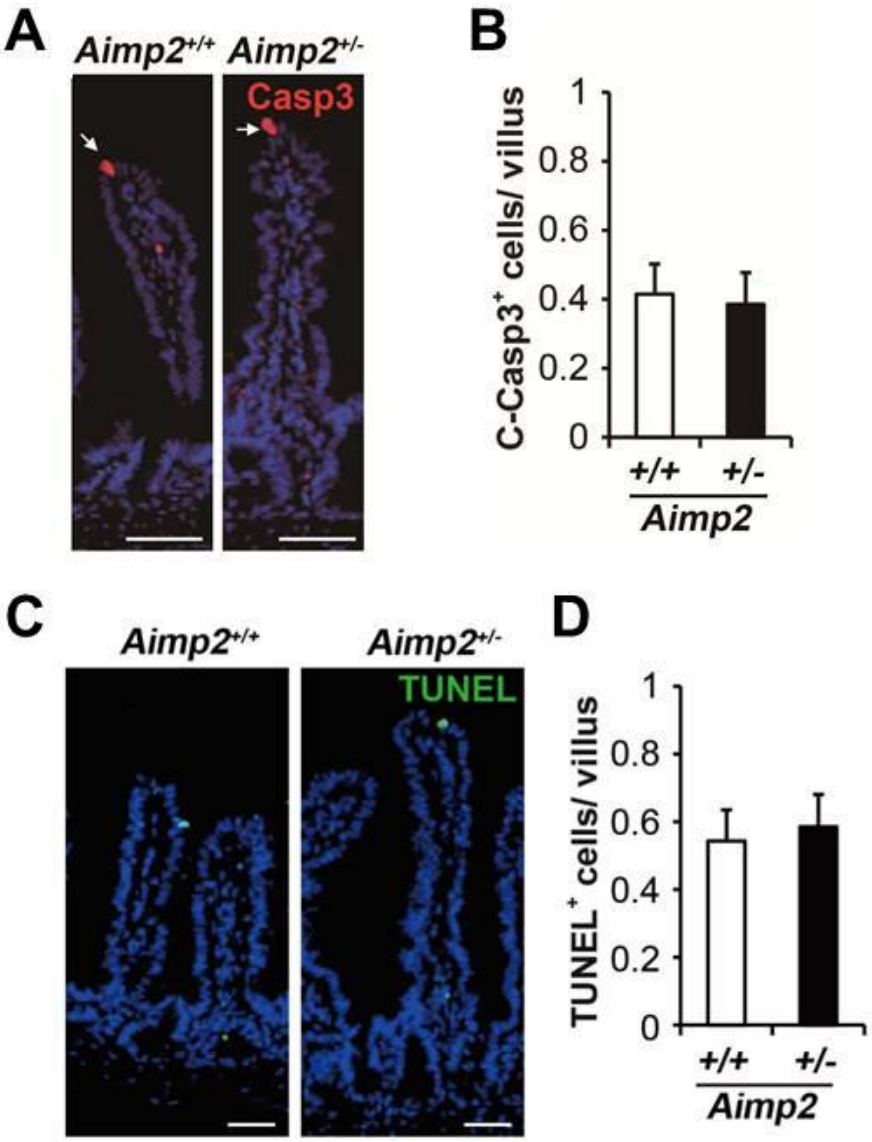
A
Aimp2+/+
Aimp2+/-
Casp3
B
C-Casp3+ cells/ villus
1
0.8
0.6
0.4
0.2
0
+/+
+/-
Aimp2
C
Aimp2+/+
Aimp2+/-
TUNEL
D
TUNEL+ cells/ villus
1
0.8
0.6
0.4
0.2
0
+/+
+/-
Aimp2

AIMP2 restricts the expansion of ISCs and their niche

To investigate which types of cells are increased in *Aimp2*$^{+/-}$ intestine, I performed qRT-PCR analysis. The expression levels of goblet and enteroendocrine cell markers (*Gob5* and *Chga*) were comparable in *Aimp2*$^{+/-}$ and *Aimp2*$^{+/+}$ mice (Fig. 15*A*). Consistently, PAS/ H and chromogranin A (ChgA) staining showed that the frequency of goblet and enteroendocrine cells was not altered in *Aimp2*$^{+/-}$ mice (Fig. 16*A-D*). However, PC markers (*Mmp7* and *Lyz*) and ISC markers (*Lgr5, Olfm4* and *Msi1*) were significantly increased in *Aimp2*$^{+/-}$ intestines compared with *Aimp2*$^{+/+}$ (Fig. 15*A*), suggesting that PCs and ISCs are expanded in *Aimp2*$^{+/-}$ mice.

To determine whether hemizygous deletion of *Aimp2* resulted in the expansion of the ISC compartment, I performed PAS/H staining and immunohistochemistry for lysozyme. Consistent with the mRNA expression, the number of PCs markedly increased in *Aimp2*$^{+/-}$ intestines (5.6 ± 1.3 per crypt) compared with *Aimp2*$^{+/+}$ (3.6 ± 0.7 per crypt) (Fig. 17*A* and *B*). To directly assess the number of ISCs, I crossed *Aimp2*$^{+/-}$ mice with *Lgr5-EGFP* mice (Barker et al., 2007). Immunohistochemical analysis showed that EGFP^{+} ISCs in the crypts markedly increased in *Aimp2*$^{+/-}$:*Lgr5-EGFP* mice (*Aimp2*$^{+/+}$: 3.3 ± 0.5 vs. *Aimp2*$^{+/-}$: 5.7 ± 1.3 per crypt). Moreover, the number of BrdU^{+}:EGFP^{+} ISCs significantly increased in the *Aimp2*$^{+/-}$:*Lgr5-EGFP* crypts (*Aimp2*$^{+/+}$: 0.9 ± 0.4 vs. *Aimp2*$^{+/-}$: 2.5 ± 0.7 per crypt) (Fig. 18*A*

and *B*), showing that two alleles of *Aimp2* are required to suppress the expansion of ISC compartments in the crypt.

Figure 15. mRNA expressions of different intestinal cell lineage markers. The goblet cell marker (*Gob5*), The enteroendocrine cell marker (*Chga*), The Paneth cell markers (*Mmp7.Lyz*) and The intestinal stem cell markers (*Lgr5, Olfm4, Msi1*) are tested in 6-week-old *Aimp2*$^{+/+}$ (n = 4) and *Aimp2*$^{+/-}$ (n = 5) intestinal epithelium.

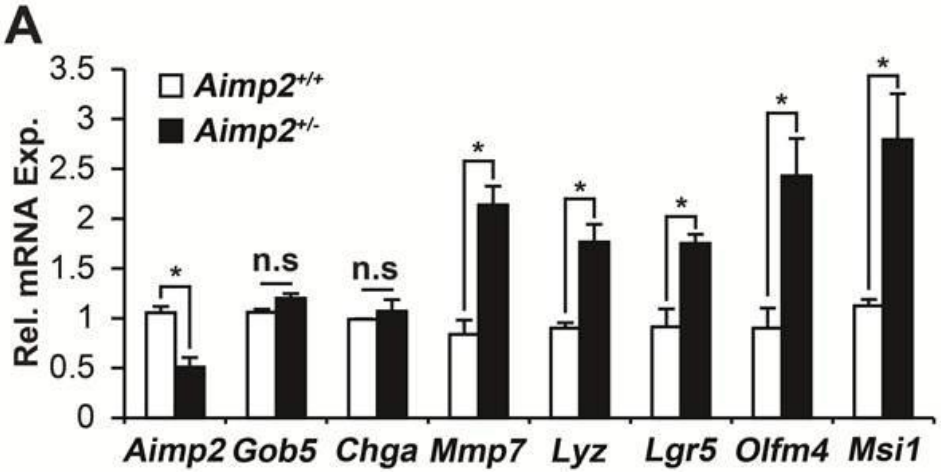
A
Rel. mRNA Exp.
3.5
3
2.5
2
1.5
1
0.5
0
Aimp2+/+
Aimp2+/-
*
n.s
n.s
*
*
*
*
*
Aimp2
Gob5
Chga
Mmp7
Lyz
Lgr5
Olfm4
Msi1

Figure 16. The differentiation of goblet and enteroendocrine cells are not affected by AIMP2 reduction (A) Representative PAS/H staining in intestinal sections (ileum) from 6-week-old *Aimp2*$^{+/+}$ and *Aimp2*$^{+/-}$ littermates. (B) Quantification of PAS^{+} cells in *Aimp2*$^{+/+}$ (n = 3) and *Aimp2*$^{+/-}$ villi (n = 3). (C) Representative images of immunohistochemistry with an anti-chromogranin A antibody in intestinal sections (ileum) from 6-week-old *Aimp2*$^{+/+}$ and *Aimp2*$^{+/-}$ littermates. (D) Quantification of chromogranin A^{+} cells in *Aimp2*$^{+/+}$ (n = 3) and *Aimp2*$^{+/-}$ villi (n = 3). The cells were counted in at least 30 well-oriented villi for each mouse. Scale bar, 50 μm. Student *t*-test was performed, and data were presented as the mean ± standard error of the mean. **P* < 0.01.

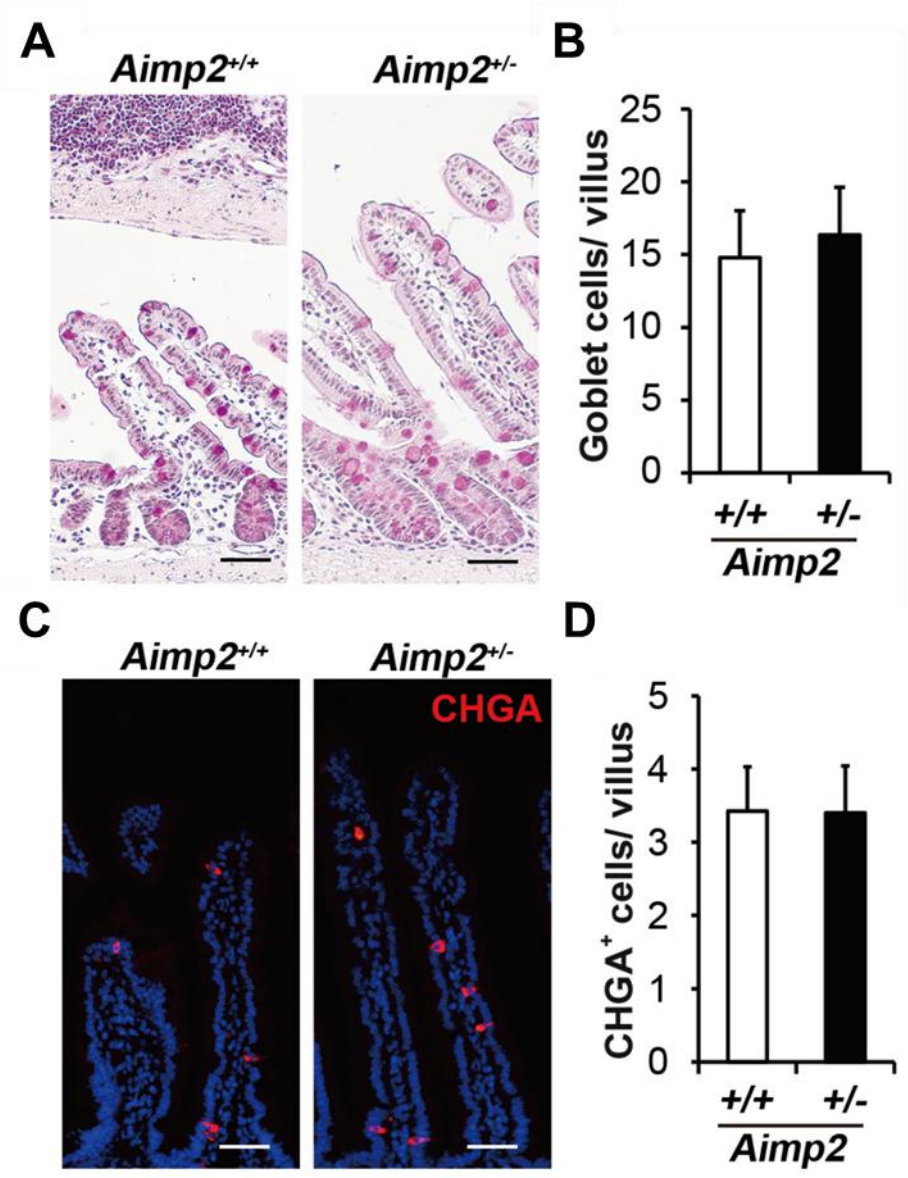
A
Aimp2+/+
Aimp2+/-
B
Goblet cells/ villus
25
20
15
10
5
0
+/+
+/-
Aimp2
C
Aimp2+/+
Aimp2+/-
CHGA
D
CHGA+ cells/ villus
5
4
3
2
1
0
+/+
+/-
Aimp2

Figure 17. Paneth cells are increased in *Aimp2*$^{+/-}$ intestine (A) PAS/H staining and immunohistochemical staining of Lysozyme in ileums. The crypts are outlined by black or white dashed lines. (B) Quantification of lysozyme^{+} cells in *Aimp2*$^{+/+}$ (n = 3) and *Aimp2*$^{+/-}$ crypts (n = 3). At least 30 well-oriented crypts were analyzed on 3-4 slides per mouse. Scale bar, 50 μm. Student *t*-test was applied, and data are the mean ± SEM. *$P < 0.01$.

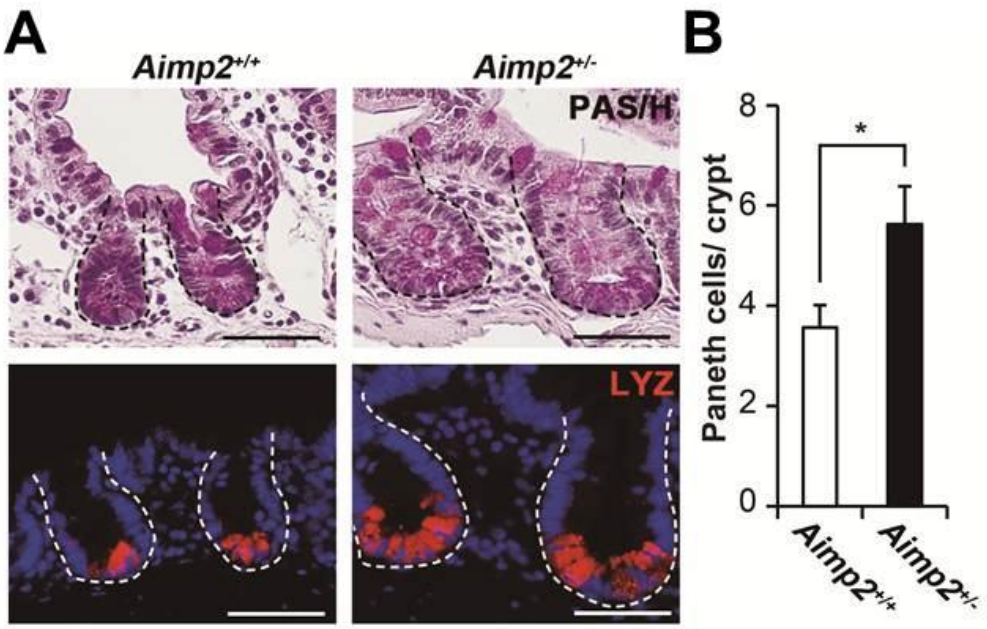
A
Aimp2+/+
Aimp2+/-
PAS/H
LYZ
B
Paneth cells/ crypt
8
6
4
2
0
*
Aimp2+/+
Aimp2+/-

Figure 18. Expansion of intestinal stem cell compartment in *Aimp2*$^{+/-}$ mice (A) Immunohistochemical staining (A) and quantification (B) of GFP and BrdU in 6-week-old *Aimp2*$^{+/+}$:*Lgr5-EGFP* (n = 3) and *Aimp2*$^{+/-}$:*Lgr5-EGFP* (n = 3) ileums. The GFP^{+} ISCs are outlined by white dashed lines. Arrow head and arrow indicate BrdU^{-}:GFP^{+} ISCs and BrdU^{+}:GFP^{+} ISCs, respectively. At least 30 well-oriented crypts were analyzed on 3-4 slides per mouse. Scale bar, 50 μm. Student *t*-test was applied, and data are the mean ± SEM. **P* < 0.01.

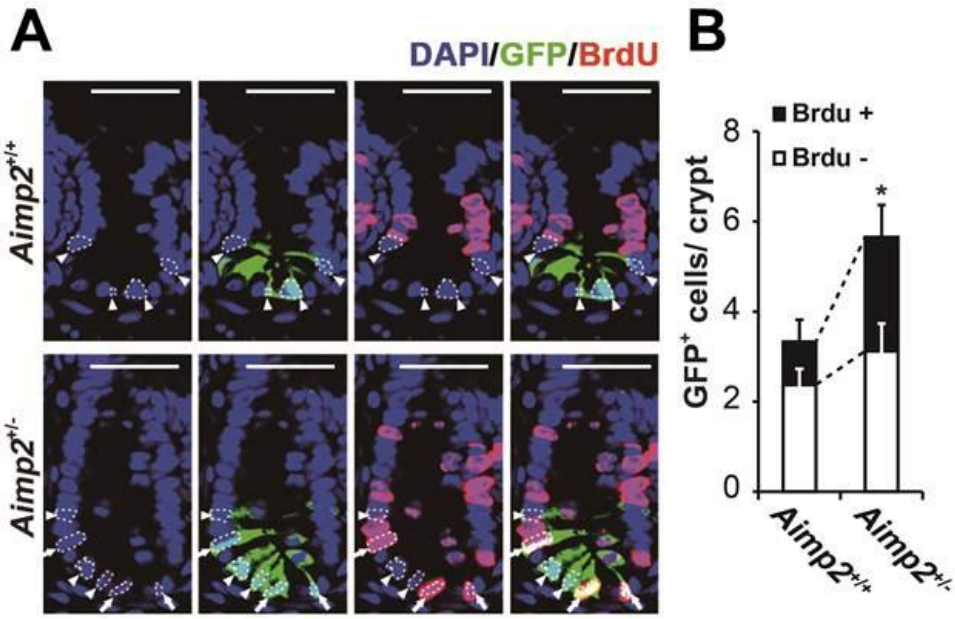
A
DAPI/GFP/BrdU
Aimp2+/+
Aimp2+/-
B
Brdu +
Brdu -
GFP+ cells/ crypt
8
6
4
2
0
*
Aimp2+/+
Aimp2+/-

AIMP2 inhibits Wnt/β-catenin signaling in the intestinal epithelium

To investigate the mechanism by which AIMP2 restricts the expansion of the ISC compartment, I first examined the target genes of known AIMP2-associated signaling pathways (Choi et al., 2009a; Han et al., 2008; Kim et al., 2003) such as FBP (*Usp29* and *Cdkn1a*), NF-κB (*Tnf*, *Gadd45b*, and *Ciap2*), and p53 (*Puma*, *Wip1*, and *Phlda3*) (Brady et al., 2011; Guma et al., 2011; Zhang and Chen, 2013). However, there were no significant differences in the expressions between the *Aimp2*$^{+/-}$ and *Aimp2*$^{+/+}$ intestine (data not shown), suggesting that the phenotype in *Aimp2*$^{+/-}$ intestine may not be caused by alteration of previously reported signaling.

At the crypt base, Wnt/β-catenin signaling governs the maintenance of ISCs and PCs, and uncontrolled activation of Wnt/β-catenin signaling leads to the expansion of ISC compartments (Andreu et al., 2005; Koo et al., 2012). Because the number of ISCs and PCs increased in *Aimp2*$^{+/-}$ mice, I investigated whether Wnt/β-catenin signaling was enhanced in the *Aimp2*$^{+/-}$ intestine. Consistent with increased levels of Wnt/β-catenin target genes (*Axin2*, *C-myc*, *Cd44*) (Fig. 19*A*), immunohistochemical analysis also showed that CD44 and C-MYC-expressing cells markedly increased in *Aimp2*$^{+/-}$ crypts (Fig. 19*B* and *C*). Moreover, increased protein levels of non-phosphorylated β-catenin, AXIN2 and NKD1 also showed the enhanced Wnt/β-catenin signaling in *Aimp2*$^{+/-}$ IECs (Fig. 19*D* and *E*) suggesting that AIMP2

inhibits Wnt/β-catenin signaling.

Figure 19. Increased Wnt/β-catenin signaling in *Aimp2*$^{+/-}$ mice (A) mRNA expressions of Wnt/β-catenin target genes in 6-week-old *Aimp2*$^{+/+}$ (n = 6) and *Aimp2*$^{+/-}$ (n = 6) intestinal epithelium. (B–C) Immunohistochemical staining of CD44 (B) and C-MYC (C) in ileums. (D-E) Immunoblotting (D) and quantitative densitometry (E) of whole cell extracts from 6-week-old *Aimp2*$^{+/+}$ (n = 4) and *Aimp2*$^{+/-}$ (n = 4) IECs. The crypts are outlined by white dashed lines. Scale bar, 50 μm. Student *t*-test was applied, and data are the mean ± SEM. **P* < 0.01.

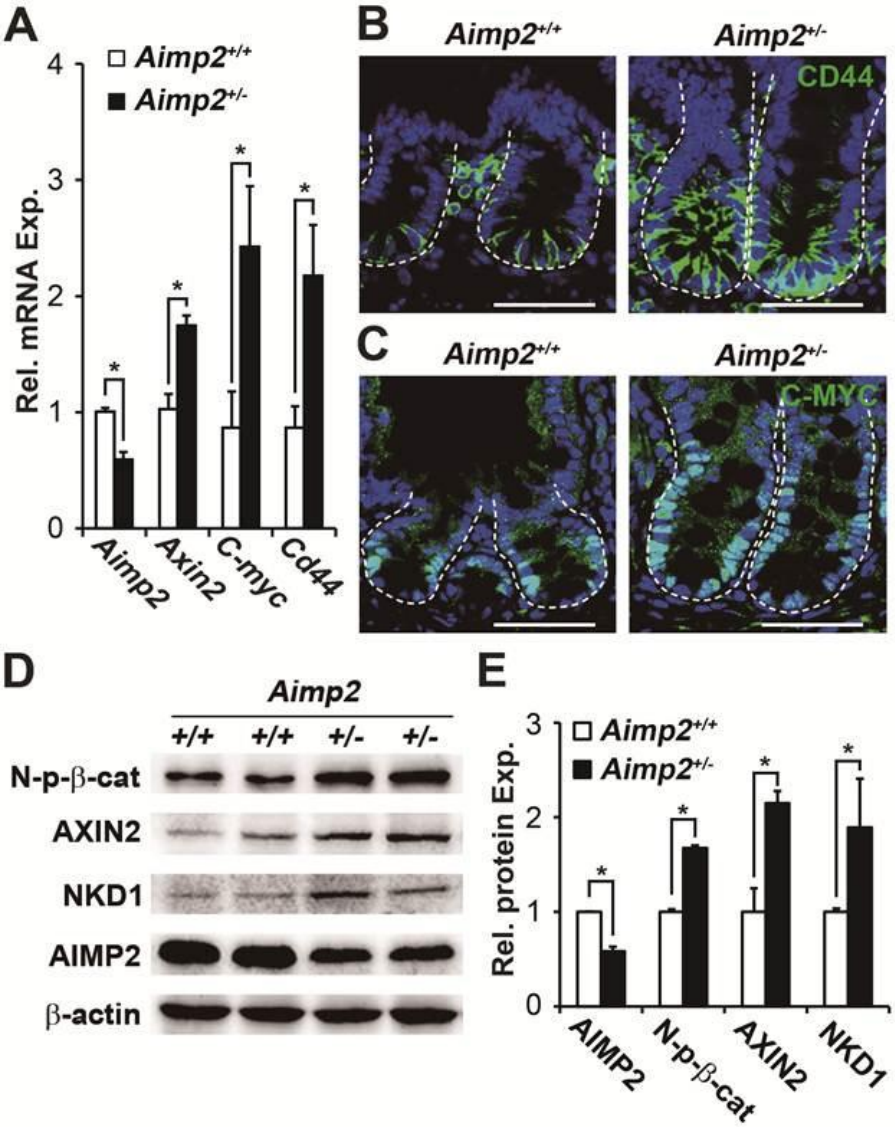
A
Aimp2+/+
Aimp2+/-
Rel. mRNA Exp.
0
1
2
3
4
Aimp2
Axin2
C-myc
Cd44
B
Aimp2+/+
Aimp2+/-
CD44
C
Aimp2+/+
Aimp2+/-
C-MYC
D
Aimp2
+/+
+/+
+/-
+/-
N-p-β-cat
AXIN2
NKD1
AIMP2
β-actin
E
Aimp2+/+
Aimp2+/-
Rel. protein Exp.
0
1
2
3
AIMP2
N-p-β-cat
AXIN2
NKD1

AIMP2 binds to Dishevelled to interrupt Dvl-Axin interaction

To investigate how AIMP2 inhibits Wnt/β-catenin signaling, I performed an *in vitro* binding assay with the major components of the canonical Wnt pathway. Intriguingly, I found that DVL bound to AIMP2 (Fig. 20*A*). I then examined whether AIMP2 co-localized with DVL. Ectopic expression of AIMP2 alone showed its diffused localization in the cytoplasm. However, co-expression of AIMP2 with DVL1 led to co-localization of AIMP2 with DVL1 as a puncta (Fig. 20*B*). Since DVL interact with AXIN in Wnt signaling cascade (Kishida et al., 1999; Schwarz-Romond et al., 2007), the binding of AIMP2 and DVL might disrupt the interaction between DVL1 and AXIN. To test this possibility, I performed co-immunoprecipitation. As expected, endogenous AIMP2 interacted with endogenous DVL1, and reduction of AIMP2 significantly increased the DVL1-AXIN1 interaction in MEFs (Fig. 21*A* and *B*). I confirmed the endogenous interaction by co-immunoprecipitation using freshly isolated *Aimp2*$^{+/+}$ and *Aimp2*$^{+/-}$ IECs (Fig. 21*C* and *D*). These results suggest that AIMP2 disrupts DVL-AXIN interaction by competing with AXIN.

Figure 20. AIMP2 associates with Dvl (A-B) HCT116 cells were transfected with plasmids as indicated. Immunoprecipitation (A) using an anti-HA antibody and immunocytochemical staining (B) using anti-HA and GFP antibody. A2-GFP represents AIMP2-GFP. Scale bar, 10 μm. At least 3 independent experiments were performed.

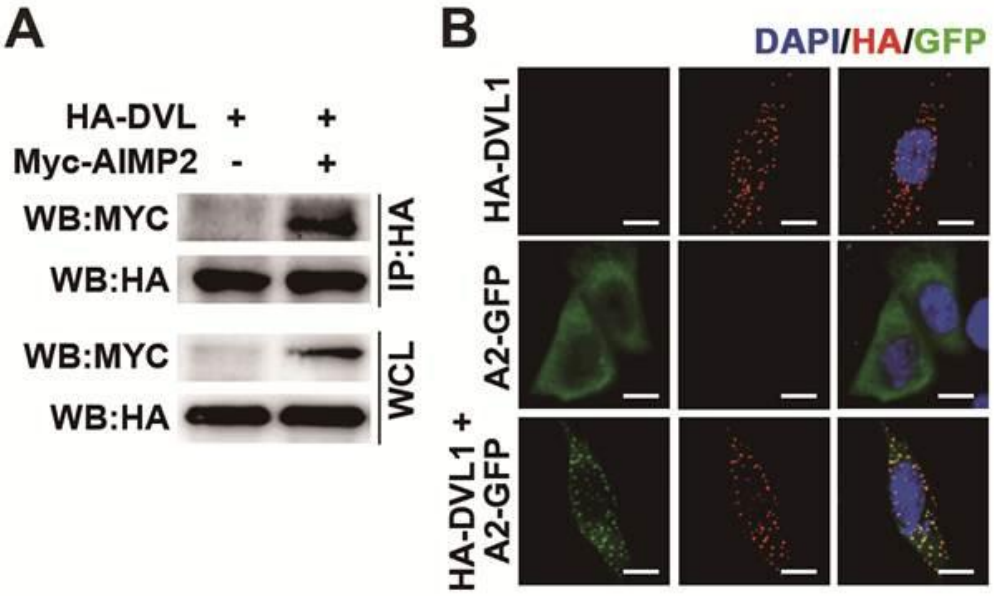
A
HA-DVL + +
Myc-AIMP2 - +
WB:MYC
WB:HA
IP:HA
WB:MYC
WB:HA
WCL
B
DAPI/HA/GFP
HA-DVL1
A2-GFP
HA-DVL1 +
A2-GFP

Figure 21. AIMP2 interrupts DVL-AXIN interaction (A-B) Immunoprecipitation analysis (A) and Quantitative densitometry of the co-IPed AXIN1 (B) using whole cell extracts from *Aimp2*$^{+/+}$ and *Aimp2*$^{-/-}$ MEFs treated with Wnt3a for 24 hr. (C-D) Immunoprecipitation analysis (C) and Quantitative densitometry of the co-IPed AXIN1 (D) using whole cell extracts from 6-week-old *Aimp2*$^{+/+}$ (n = 4) and *Aimp2*$^{+/-}$ (n = 4) IECs. Student *t*-test was applied, and data are the mean ± SEM. **P* < 0.01. At least 3 independent experiments were performed.

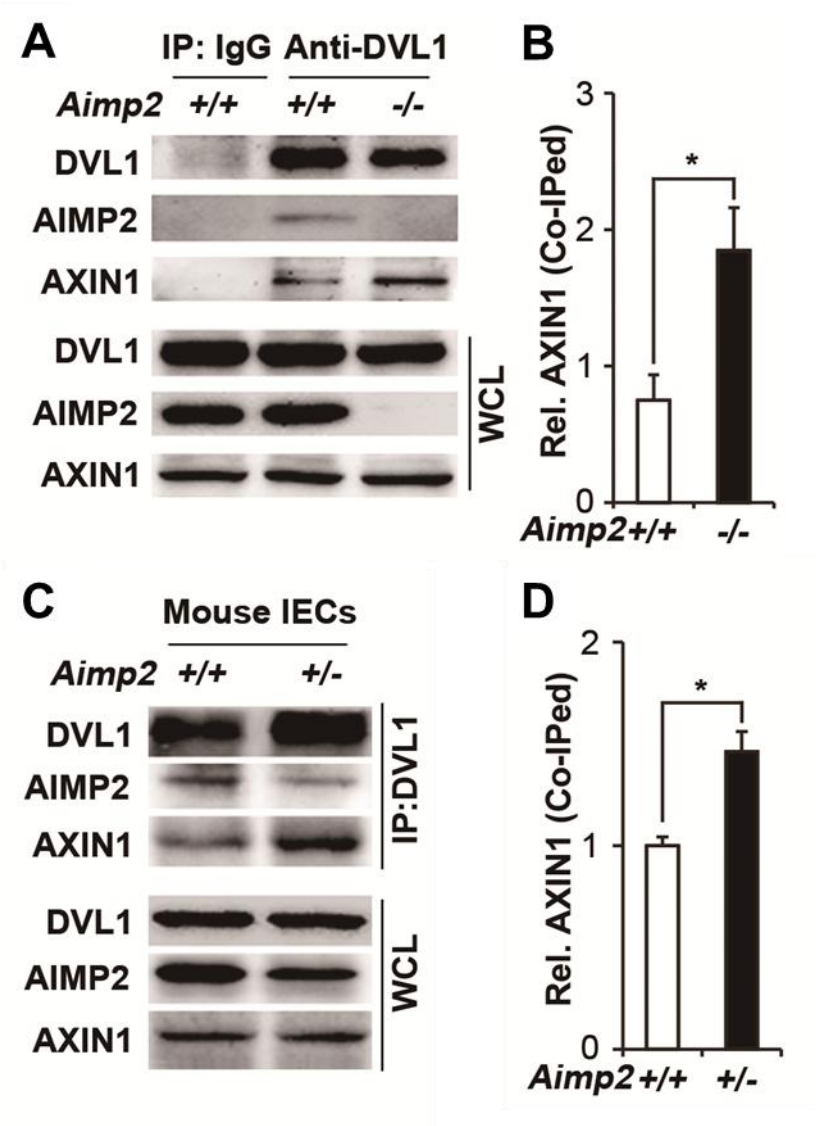
A
IP: IgG
Anti-DVL1
Aimp2 +/+ +/+ -/-
DVL1
AIMP2
AXIN1
DVL1
AIMP2
AXIN1
WCL
B
Rel. AXIN1 (Co-IPed)
3
2
1
0
*
Aimp2 +/+ -/-
C
Mouse IECs
Aimp2 +/+ +/-
DVL1
AIMP2
AXIN1
IP:DVL1
DVL1
AIMP2
AXIN1
WCL
D
Rel. AXIN1 (Co-IPed)
2
1
0
*
Aimp2 +/+ +/-

AIMP2 inhibits Wnt/β-catenin signaling

Because AIMP2 inhibited the DVL-AXIN interaction, I tested whether AIMP2 negatively regulated Wnt/β-catenin signaling. Overexpression of AIMP2 inhibited the activity of TOPflash, a reporter for Wnt/β-catenin signaling (Fig. 22*A*), the accumulation of non-phosphorylated β-catenin, the induction of AXIN2 and NKD1 after Wnt3a stimulation (Fig. 22*B*) and the expression of the Wnt/β-catenin target genes, *AXIN2 and NKD1* (Fig. 22*C*). Conversely, *AIMP2* knockdown further augmented Wnt3a-mediated increase of the TOPflash activity (Fig. 22*D*), the accumulation of non-phosphorylated β-catenin and the target gene expressions (Fig. 22*E* and *F*). Consistently, ablation of *Aimp2* in MEFs (Fig. 23*A* and *B)* increased the TOPflash activity with or without Wnt3a stimulation (Fig. 23*C*). Blockade of Wnt ligand secretion by a porcupine inhibitor, IWP4 (Chen et al., 2009), revealed that the increased Wnt/β-catenin signaling in *Aimp2*$^{-/-}$ MEFs depends on Wnt ligand administration (Fig. 23*D*), suggesting that *Aimp2*$^{-/-}$ MEFs were more sensitive to Wnt ligands than *Aimp2*$^{+/+}$ MEFs**.** Taken together, these results show that AIMP2 inhibits Wnt/β-catenin signaling by disrupting the interaction between DVL and AXIN.

Previous studies suggested that AIMP2 is involved in ubiquitination-dependent degradation of TRAF2 and p53 (Choi et al., 2009a; Han et al., 2008) by the direct interaction. Thus I tested whether AIMP2 modulates the Wnt/β-catenin signaling by ubiquitination of

DVL1. When DVL1 was overexpressed alone or with AIMP2, there was no significant difference in DVL1 level (Fig. 20*A* and *B*). Moreover, the protein levels of DVL1 in MEFs and *Aimp2*$^{+/+}$, *Aimp2*$^{+/-}$ and even *Aimp2*$^{-/-}$ IECs were comparable, suggesting that the inhibitory role of AIMP2 on Wnt/β-catenin signaling may not depend on DVL1 degradation (Fig. 24*A*-*C*).

Since AIMP2 associates with several E3-ligases such as IAP-1 (Choi et al., 2009a) and MDM2 (Han et al., 2008), I further tested whether AIMP2 affects the ubiquitination of β-catenin independently of destruction complex. When HeLa cells were treated with GSK-3β inhibitor (CHIR99021), AIMP2 overexpression did not induce the ubiquitination of β-catenin. In contrast, AIMP2 readily induced the ubiquitination of β-catenin when cells were stimulated with Wnt3a (Fig. 25*A*), suggesting that AIMP2 inhibits upstream of GSK-3β in Wnt/β-catenin signaling. Consistently, in the presence of CHIR99021, Top-flash activity (Fig. 25*B* and *C*) and *AXIN2* mRNA expression (Fig. 25*D* and *E*) were not affected by AIMP2 level. Therefore, I concluded that the regulatory role of AIMP2 in Wnt/β-catenin signaling is mainly dependent on the disruption of DVL-AXIN interaction, not the direct ubiquitination.

Figure 22. AIMP2 inhibits Wnt/β-catenin signaling (A-C) TOPflash analysis (A), immunoblotting (B) and qPCR analysis (C) of whole cell extracts from HeLa cells transfected with Empty vector (EV) or AIMP2 expression vector, and treated with Wnt3a for 24 hr. (D-F) TOPflash analysis (D), immunoblotting (E) and qPCR analysis (F) of HeLa cells transfected with scramble (Scr) or AIMP2 siRNAs and treated with Wnt3a for 24 hr. Student *t*-test (C) or ANOVA (F, I, J, K) was performed, and data were presented as the mean ± standard error of the mean. *$P < 0.01$. At least 3 independent experiments were performed.

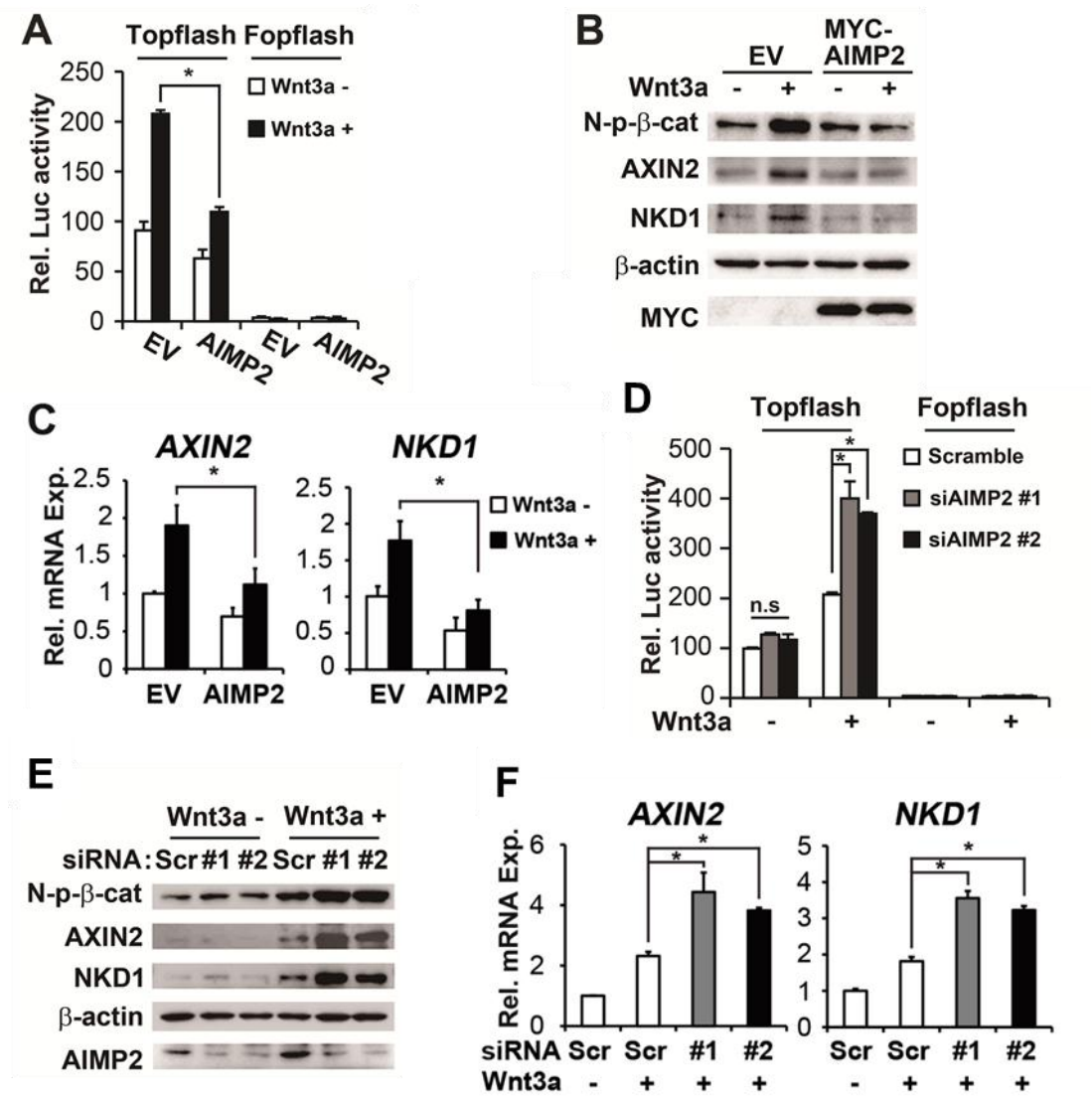
A
Topflash Fopflash
Rel. Luc activity
250
200
150
100
50
0
Wnt3a -
Wnt3a +
EV
AIMP2
EV
AIMP2
B
EV
MYC-AIMP2
Wnt3a - + - +
N-p-β-cat
AXIN2
NKD1
β-actin
MYC
C
AXIN2
NKD1
Rel. mRNA Exp.
2.5
2
1.5
1
0.5
0
Wnt3a -
Wnt3a +
EV
AIMP2
EV
AIMP2
D
Topflash
Fopflash
Rel. Luc activity
500
400
300
200
100
0
Scramble
siAIMP2 #1
siAIMP2 #2
n.s
Wnt3a - + - +
E
Wnt3a -
Wnt3a +
siRNA: Scr #1 #2 Scr #1 #2
N-p-β-cat
AXIN2
NKD1
β-actin
AIMP2
F
AXIN2
NKD1
Rel. mRNA Exp.
6
4
2
0
5
4
3
2
1
0
siRNA Scr Scr #1 #2
Wnt3a - + + +
Scr Scr #1 #2
- + + +

Figure 23. Ablation of *Aimp2* in MEFs increases Wnt/β-catenin signaling. (A-B) The expression of *Aimp2* mRNA (A) and AIMP2 protein (B) was analyzed with qRT-PCR and immunoblotting in *Aimp2*$^{+/+}$, *Aimp2*$^{+/-}$, and *Aimp2*$^{-/-}$ MEFs. (C) The TOPflash activity were measured in *Aimp2*$^{+/+}$, *Aimp2*$^{+/-}$, and *Aimp2*$^{-/-}$ MEFs treated with Wnt3a for 24 hr. (D) The expression of *Axin2* mRNA in *Aimp2*$^{+/+}$, *Aimp2*$^{+/-}$, and *Aimp2*$^{-/-}$ MEFs. The cells were pretreated with porcupine inhibitor (IWP4, Stemgent) for 24 hr, and stimulated with Wnt3a for 12 hr in the presence of IWP4. ANOVA (C,D) was performed, and data were presented as the mean ± standard error of the mean. *$P < 0.01$. At least 3 independent experiments were performed.

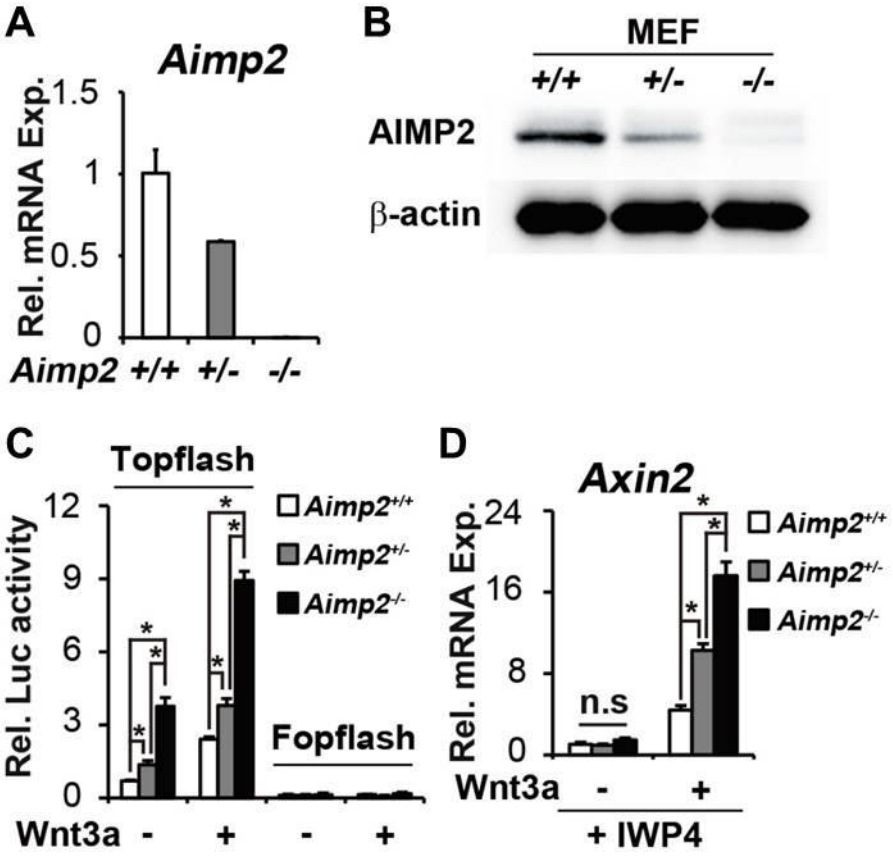
A
Aimp2
Rel. mRNA Exp.
1.5
1
0.5
0
Aimp2 +/+ +/- -/-
B
MEF
+/+ +/- -/-
AIMP2
β-actin
C
Topflash
Fopflash
Rel. Luc activity
12
9
6
3
0
Aimp2+/+
Aimp2+/-
Aimp2-/-
Wnt3a - + - +
D
Axin2
Rel. mRNA Exp.
24
16
8
0
n.s
Wnt3a - +
+ IWP4

Figure 24. AIMP2 does not affect the protein level of DVL (A-C) The level of endogenous DVL1 protein was analyzed with immunoblotting in *Aimp2*$^{+/+}$, *Aimp2*$^{+/-}$, and *Aimp2*$^{-/-}$ MEFs (A), 6-week-old *Aimp2*$^{+/+}$, *Aimp2*$^{+/-}$ intestinal epithelial cells (B), and postnatal day 0 *Aimp2*$^{+/+}$, *Aimp2*$^{+/-}$, and *Aimp2*$^{-/-}$ intestinal epithelial cells (C). At least 3 independent experiments were performed.

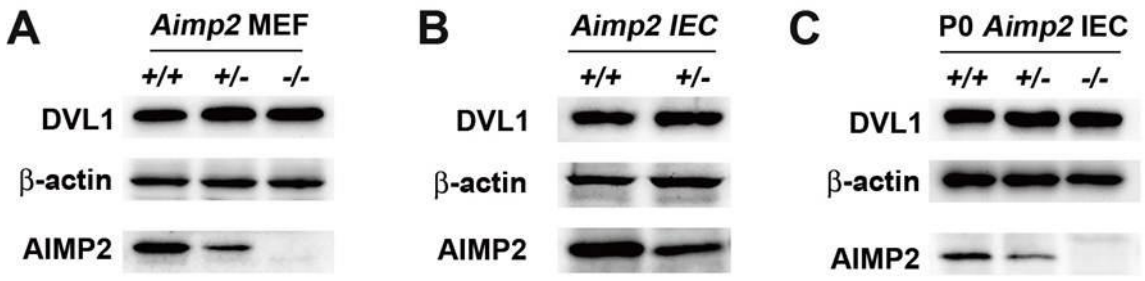
A
Aimp2 MEF
+/+ +/- -/-
DVL1
β-actin
AIMP2
B
Aimp2 IEC
+/+ +/-
DVL1
β-actin
AIMP2
C
P0 Aimp2 IEC
+/+ +/- -/-
DVL1
β-actin
AIMP2

Figure 25. AIMP2 does not affect the ubiquitination of β-catenin by destruction complex.

(A) HeLa cells were transfected with plasmids as indicated, and protein was immunoprecipitated using anti-β-catenin antibody and immunoblotted using indicated antibodies. Black arrow heads indicate 100kda. (B,D) HeLa cells were transfected with Empty vectors (EV) or AIMP2 overexpression vectors and in the absence or presence of GSK-3β inhibitor (CHIR99021, Stemgent), the Topflash activity (B) or expression of *AXIN2* (D) was measured. (C,E) the Topflash activity (C) and the expression of *Axin2* (E) in *Aimp2*$^{+/+}$ and *Aimp2*$^{-/-}$ MEFs was also analyzed. Student *t*-test was performed, and data were presented as the mean ± standard error of the mean. At least 3 independent experiments were performed.

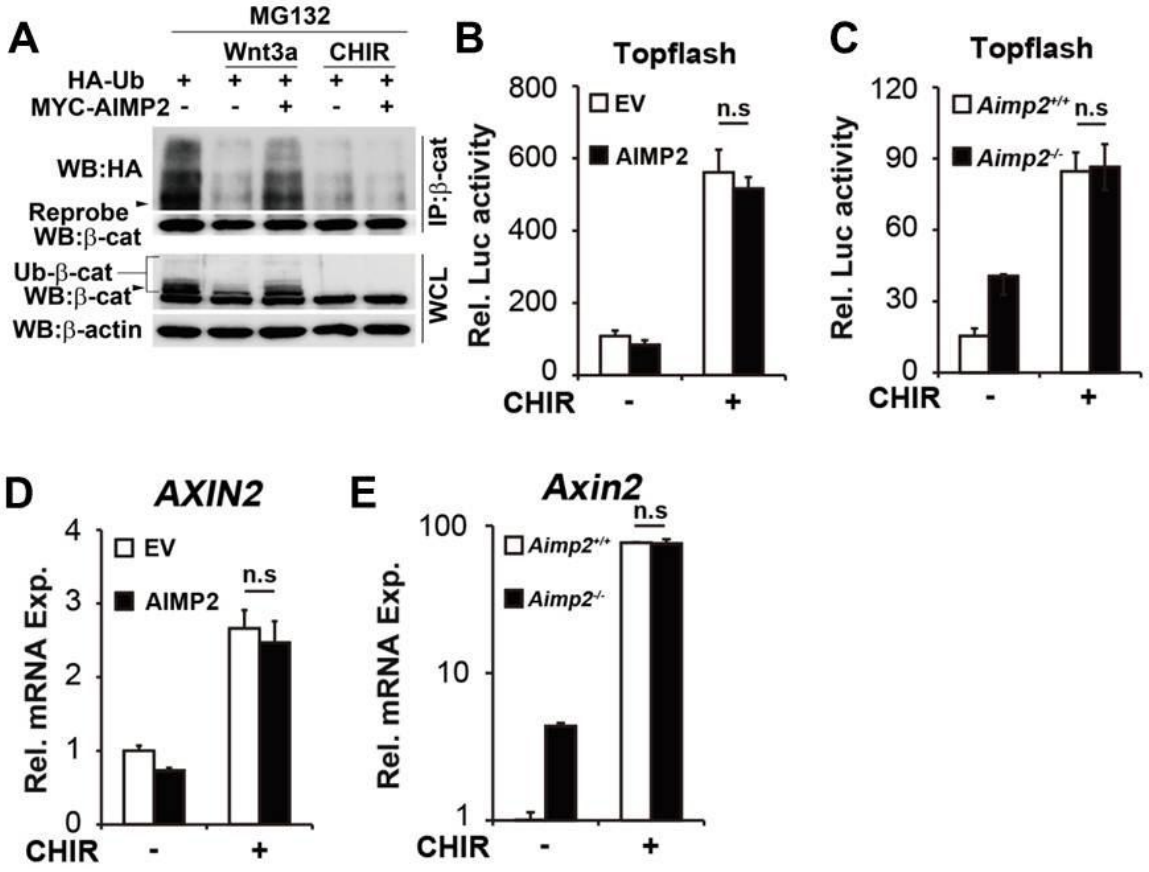
A
MG132
Wnt3a
CHIR
HA-Ub + + + + +
MYC-AIMP2 - - + - +
WB:HA
Reprobe
WB:β-cat
IP:β-cat
Ub-β-cat
WB:β-cat
WB:β-actin
WCL
B
Topflash
Rel. Luc activity
800
600
400
200
0
EV
AIMP2
n.s
CHIR - +
C
Topflash
Rel. Luc activity
120
90
60
30
0
Aimp2+/+
Aimp2-/-
n.s
CHIR - +
D
AXIN2
Rel. mRNA Exp.
4
3
2
1
0
EV
AIMP2
n.s
CHIR - +
E
Axin2
Rel. mRNA Exp.
100
10
1
Aimp2+/+
Aimp2-/-
n.s
CHIR - +

***Aimp2* gene dosages modulate the sensitivity of Wnt/β-catenin signaling**

On the basis of the data from the *Aimp2*$^{+/-}$ intestine, I speculated that *Aimp2* gene dosage is important for inhibitory role of AIMP2 in Wnt/β-catenin signaling. Indeed, compared to *Aimp2*$^{+/+}$, *Aimp2*$^{+/-}$ MEFs showed increased TOPflash activity and expressed higher levels of *Axin2*. In addition, the increase was further augmented in *Aimp2*$^{-/-}$ MEFs (Fig. 23*C* and *D*), suggesting that hemizygous expression of AIMP2 is insufficient to inhibit Wnt/β-catenin signaling. To further examine the dosage effect of AIMP2, I measured effective concentration (EC) 50 of Wnt3a using MEFs. As expected, the EC50 significantly decreased when *Aimp2* dosage reduced (Fig. 26*A*)

To confirm the dosage effects of AIMP2 in Wnt/β-catenin signaling, I performed organoid formation assays (Sato et al., 2009) in the presence of Roof plate-specific spondin 1 (R-spondin-1) using IECs from E18.5 *Aimp2*$^{+/+}$, *Aimp2*$^{+/-}$, and *Aimp2*$^{-/-}$ mouse embryos. Binding of R-spondin-1 to LGR4/5 inhibits the RNF43 and ZNRF3 E3 ligases and activates Wnt/β-catenin signaling in ISCs (de Lau et al., 2014). On day 3 of culture, the formation of intestinal organoids was negatively correlated with *Aimp2* gene dosage, especially at very low concentrations of R-spondin-1 (Fig. 27*A* and *B*). However, in the absence of R-spondin-1, no living organoids were present, regardless of genotype, suggesting that AIMP2 plays an inhibitory role in Wnt/β-catenin signaling downstream of RNF43 and ZNRF3.

Consistently, the expression of Wnt/β-catenin target genes and ISC markers (Fig. 28*A*), the proliferation (Fig. 28*B* and *C*) and the growth (Fig. 29*A* and *B*) of organoids were negatively correlated with the *Aimp2* gene dosage. Together, these results support the idea that AIMP2 inhibits the activity of Wnt/β-catenin signaling in IECs in a gene dosage-dependent manner.

Figure 26. Effects of Aimp2 gene dosage on the sensitivity to Wnt ligands (A) Dose-response curve to Wnt3a of MEFs. The cells were pretreated with porcupine inhibitor (IWP4, Stemgent) for 24 hr and stimulated with Wnt3a for 12 hr. ANOVA on effective concentration (EC) 50 value was applied, and data are the mean ± SEM. *$P < 0.01$. At least 3 independent experiments were performed.

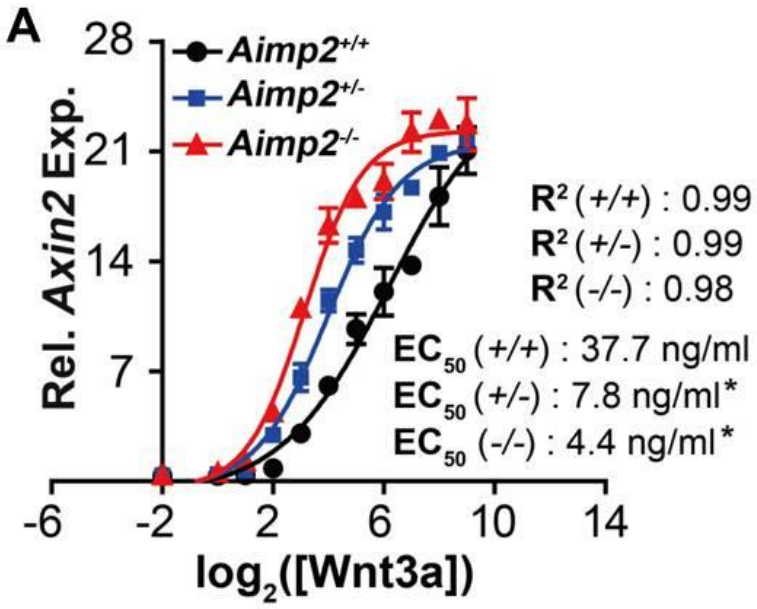
A
28
21
14
7
Rel. Axin2 Exp.
Aimp2+/+
Aimp2+/-
Aimp2-/-
R² (+/+) : 0.99
R² (+/-) : 0.99
R² (-/-) : 0.98
EC50 (+/+) : 37.7 ng/ml
EC50 (+/-) : 7.8 ng/ml*
EC50 (-/-) : 4.4 ng/ml*
-6
-2
2
6
10
14
log2([Wnt3a])

Figure 27. AIMP2 inhibits intestinal organoid formation (A-B) Stereomicroscopic images (A) and organoid formation efficiency (B) of *Aimp2*$^{+/+}$, *Aimp2*$^{+/-}$, and *Aimp2*$^{-/-}$ intestinal organoids. Arrows indicate budding of organoids. 200 crypts were seeded, and budding organoids were counted as live organoids at day 3 of culture. At least 10 organoids were analyzed for each genotype. Scale bar, 100 μm. ANOVA was performed, and data are the mean ± SEM. **P* < 0.01. At least 3 independent experiments were performed.

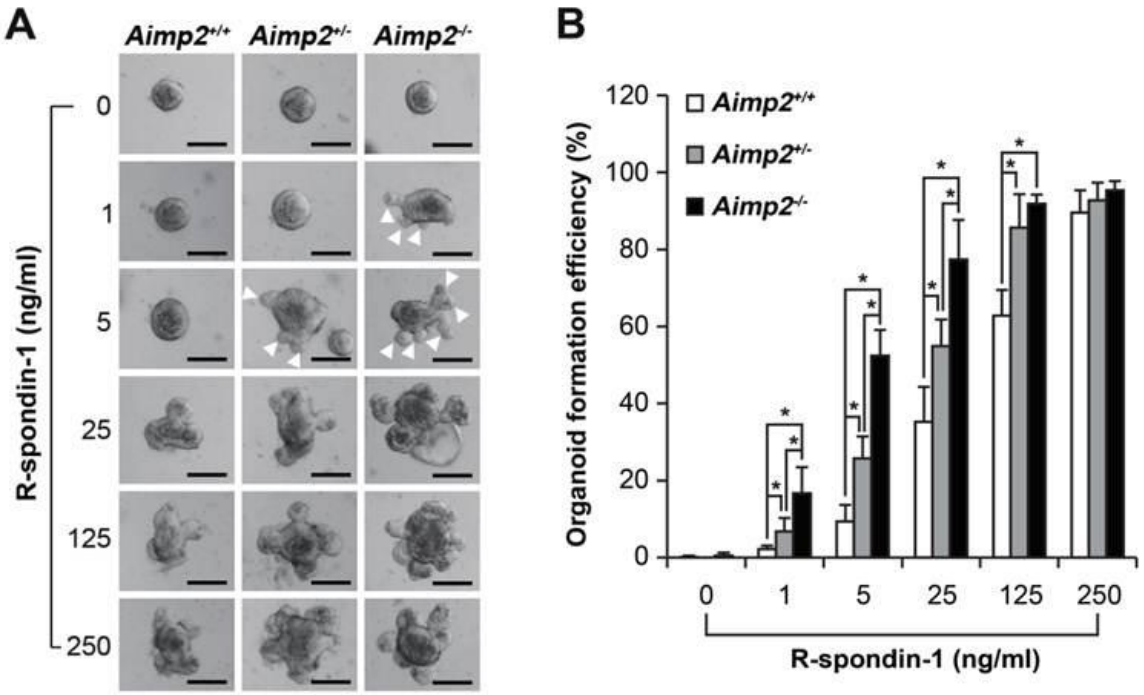
A
Aimp2+/+
Aimp2+/-
Aimp2-/-
R-spondin-1 (ng/ml)
0
1
5
25
125
250
B
Organoid formation efficiency (%)
120
100
80
60
40
20
0
Aimp2+/+
Aimp2+/-
Aimp2-/-
0
1
5
25
125
250
R-spondin-1 (ng/ml)

Figure 28. AIMP2 inhibits Wnt/β-catenin signaling in intestinal organoids (A) mRNA expressions of organoids at day 3 of culture with 25 ng/ml R-spondin-1. (B-C) Immunohistochemical staining (B) and quantification (C) of BrdU in organoids. At least 10 organoids were analyzed for each genotype. Scale bar, 100 μm. ANOVA was performed, and data are the mean ± SEM. *$P < 0.01$. At least 3 independent experiments were performed.

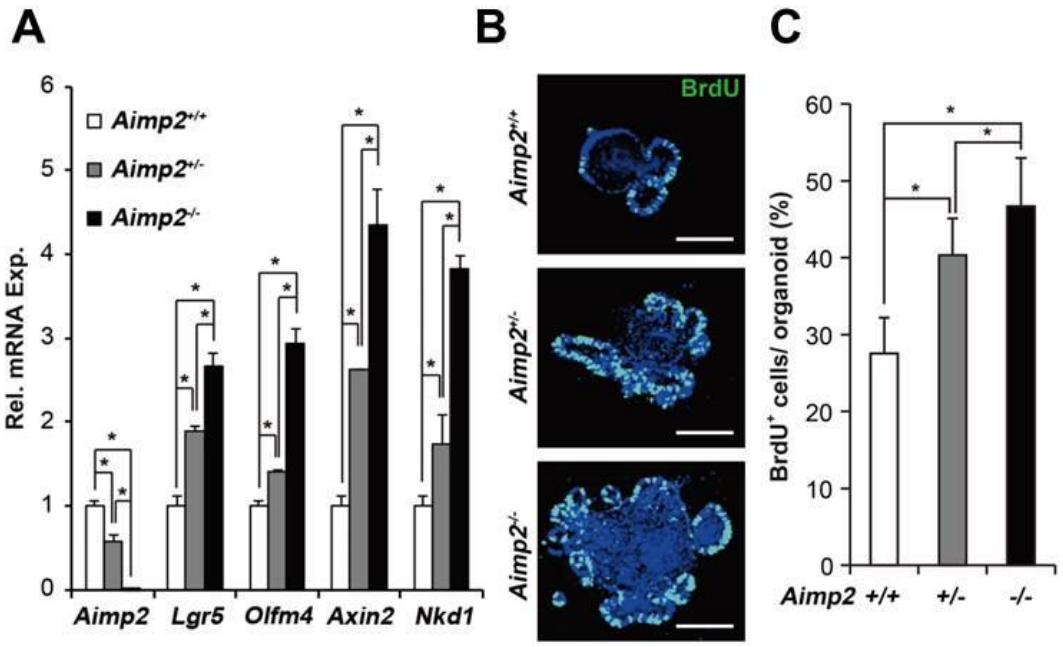
A
B
C
Rel. mRNA Exp.
Aimp2+/+
Aimp2+/-
Aimp2-/-
Aimp2
Lgr5
Olfm4
Axin2
Nkd1
BrdU
Aimp2+/+
Aimp2+/-
Aimp2-/-
BrdU+ cells/ organoid (%)
Aimp2 +/+
+/-
-/-

Figure 29. *Aimp2* gene dosage negatively correlates with organoid growth (A) The size of the organoids from *Aimp2*$^{+/+}$, *Aimp2*$^{+/-}$**,** and *Aimp2*$^{-/-}$ mice was measured by morphometric analysis of stereomicroscopic images. Organoids were cultured for 3 days with increasing concentrations of R-spondin-1. At least 10 organoids were analyzed for each genotype. (B) Stereomicroscopic images of *Aimp2*$^{+/+}$, *Aimp2*$^{+/-}$, and *Aimp2*$^{-/-}$ intestinal organoids cultured with 25 ng/ml R-spondin-1. Images were obtained at 1, 3, and 5 days of culture as indicated. Scale bar, 50 μm. ANOVA was performed, and data were presented as the mean ± standard error of the mean. *$P < 0.01$. At least 3 independent experiments were performed

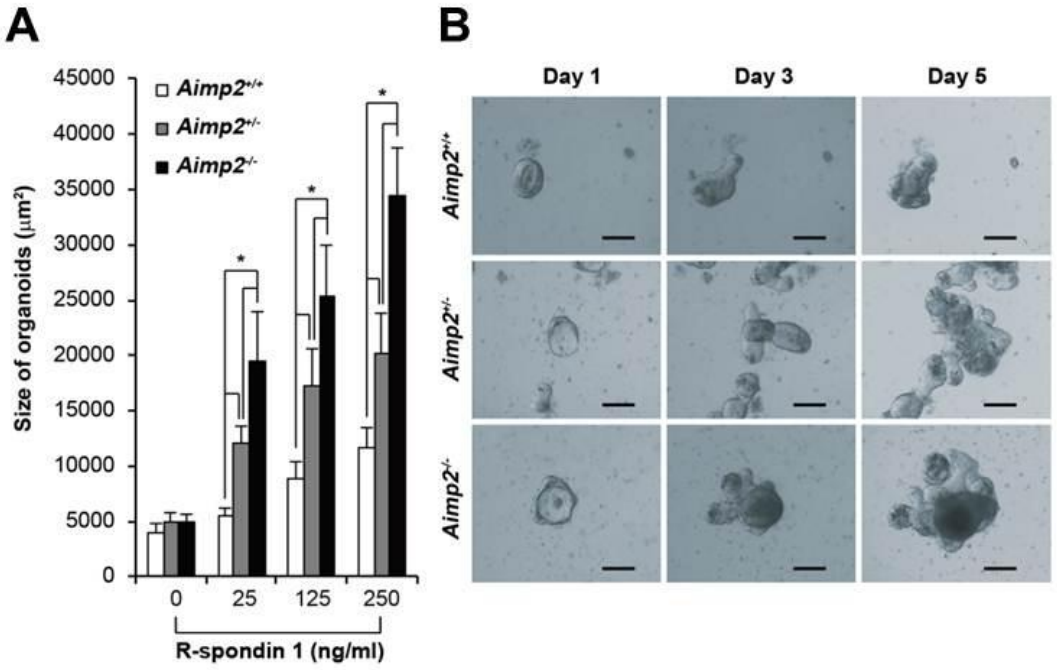
A
B
Aimp2+/+
Aimp2+/-
Aimp2-/-
Size of organoids (μm²)
45000
40000
35000
30000
25000
20000
15000
10000
5000
0
0
25
125
250
R-spondin 1 (ng/ml)
*
Day 1
Day 3
Day 5

DISCUSSION

Because an adequate level of Wnt/β-catenin signaling activity is critical for maintaining ISCs, it is important to understand the mechanism that the Wnt/β-catenin signaling activity is regulated in the intestine. Here, I show that AIMP2 binds to DVL, a key component of the Wnt/β-catenin signaling pathway and inhibits the interaction between DVL and AXIN. The inhibitory effect of AIMP2 on Wnt/β-catenin signaling is negatively correlated with the *Aimp2* gene dosage. Intriguingly, hemizygous expression of AIMP2 in the intestine was insufficient for proper control of Wnt/β-catenin signaling activity, which is pivotal in maintaining an adequate ISC pool size in the crypts. Collectively, our data show that AIMP2 is an important regulator that controls the activity of Wnt/β-catenin signaling, the ISC populations and eventually the tumorigenesis in the crypts.

In the intestinal crypts, PCs and cryptal myofibroblasts have been considered the major sources of canonical Wnt ligands (Farin et al., 2012; Sato et al., 2011). However, a recent study showed that Wnt ligands produced by unknown cellular sources are sufficient to support ISCs in the absence of PCs and myofibroblasts (San Roman et al., 2014), indicating that intestinal crypts are awash with Wnt ligands. Despite the surplus Wnt ligands in the crypts, Wnt/β-catenin signaling is not fully activated in ISCs and transit-amplifying (TA) cells, suggesting that a number of negative regulators restrict the activation of Wnt/β-catenin

signaling. Recently emerged Wnt agnonist, R-spondins likely diffuse from their unknown cellular source to activate Wnt/β-catenin signaling in surrounding epithelial cells, including ISCs. In the present study, I found that the expression of AIMP2 negatively correlated with sensitivity to R-spondin-1, suggesting that AIMP2 prevents unwanted activation of ISCs by regulating the activity of Wnt/β-catenin signaling.

Various receptors, such as receptor tyrosine kinase receptors, Toll-like receptors, and tumor necrosis factor receptors, require high-order assemblies of intracellular signaling factors (Wu, 2013). Because signalosome formation requires oligomerization, the receptors show a sigmoidal response to ligand concentration, reducing biological noise or unwanted activation. Wnt ligand-receptor binding also leads to the clustering of Frizzled and LRP6 and the polymerization of DVL. DVL self-assembles through its DIX domain and forms interaction platforms for low-affinity binding partners such as AXIN (Schwarz-Romond et al., 2007). In our study, AIMP2 competed with AXIN for binding to the DIX domain of DVL. Intriguingly, the activity of Wnt/β-catenin signaling negatively correlated with the *Aimp2* gene dosage, suggesting that AIMP2 expression level is crucial for regulation of the interaction between DVL and AXIN. Competition with AXIN might create a sharp sigmoidal response to Wnt ligands in the presence of R-spondin-1, which would provide a mechanism for reducing biological noise or unwanted activation of Wnt/β-catenin signaling in cryptic epithelial cells.

Why do *Aimp2*$^{+/-}$ crypts exhibit haploinsufficiency? AIMP2 serves as a scaffolding protein for the assembly of several different ARSs into the multi-tRNA synthetase complex (Quevillon et al., 1999). If AIMP2 is predominantly trapped in multi-synthetase complexes, a limited amount of "free" AIMP2 is available to participate in non-translational activities, such as interacting with FBP, p53, and TRAF2 (Choi et al., 2009a; Han et al., 2008; Kim et al., 2003). Thus, in *Aimp2*$^{+/-}$ mice, the amount of AIMP2 could be insufficient to support its noncanonical functions as a signaling modulator. Our data suggest another mechanism for AIMP2 haploinsufficiency, in which AIMP2 modulates Wnt/β-catenin signaling in the intestine by interfering with the DVL-AXIN interaction. On the other hand, recent studies have reported that PARKIN degrades AIMP2 in dopaminergic neurons and that disruption of PARKIN results in the accumulation of AIMP2, potentially causing neurodegenerative disease (Ko et al., 2005; Lee et al., 2013). Overall, these observations raise the intriguing possibility that the cellular level of AIMP2 is important in various pathophysiological contexts.

The key cellular events promoting tumor initiation include uncontrolled cell proliferation. LOH of *Apc*, a process directly linked to tumor initiation in *Apc*$^{Min/+}$ mice can occur in highly proliferative cells due to dysregulated cell cycle (Aoki et al., 2003; Haigis et al., 2002). Thus, the expanded ISC compartment and IEC proliferation might be responsible for increased tumorigenesis in *Aimp2*$^{+/-}$:*Apc*$^{Min/+}$ mice. These findings are consistent with

earlier report using AOM/DSS colitis-associated tumor model with increased number of polyps in the *Aimp2*$^{+/-}$ colon (Choi et al., 2009b). Furthermore, the increased ACF in *Aimp2*$^{+/-}$:*Apc*$^{Min/+}$ mice suggests that intestinal AIMP2 is essential for inhibiting adenoma initiation. Collectively, our current study revealed a critical role of AIMP2 in modulating intestinal Wnt/β-catenin signaling and tumorgenesis. Disruption of DVL-AXIN interaction by AIMP2 fine-tunes the Wnt/β-catenin signaling activity in intestinal crypts. Our observation will provide a better understanding of regulation of intestinal Wnt signaling and tumorigenesis.

Figure 30. Schematic summary for the role of AIMP2 in intestinal epithelium. In the crypt, lots of sources including Paneth cells and cryptal myofibroblast express abundant Wnt ligands. In this awash of Wnt ligands, intestinal stem cells must inhibit unwanted activation of Wnt/β-catenin signaling. AIMP2 highly expressed in the crypt and binds to DVL, a key component of the Wnt/β-catenin signaling pathway. The AIMP2-DVL binding interrupts the interaction between DVL and AXIN, resulting in inhibition of Wnt/β-catenin signaling. Our data show that AIMP2 is an important tumor-suppressor that restricts the ISC expansion by inhibiting the activity of Wnt/β-catenin signaling.

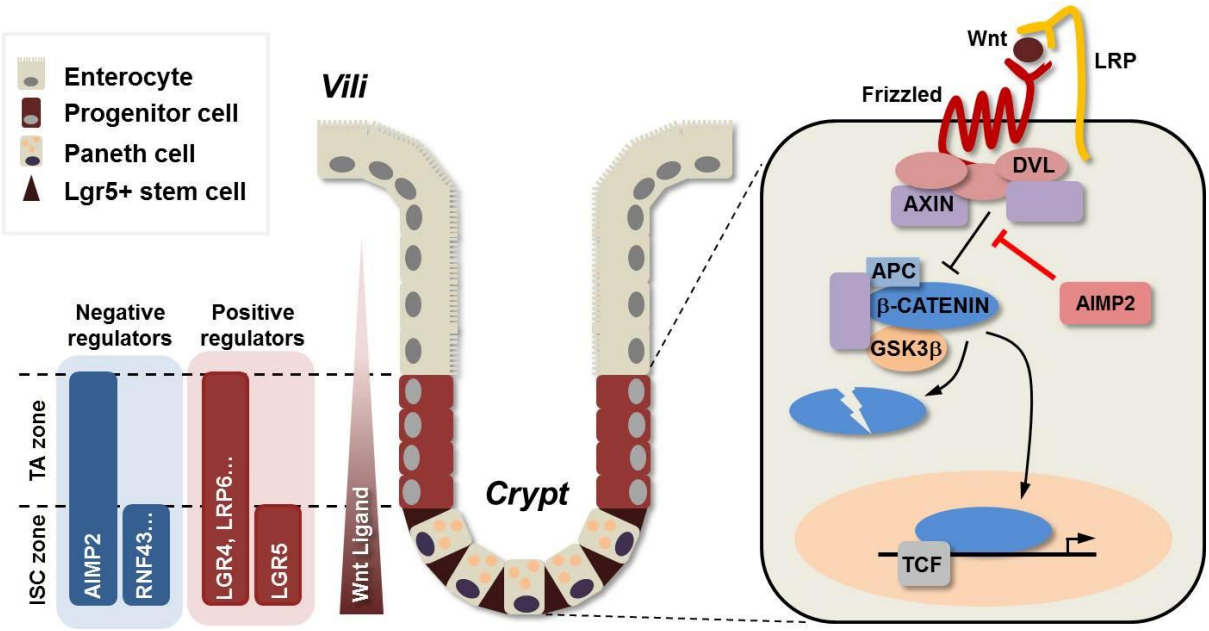
Enterocyte
Progenitor cell
Paneth cell
Lgr5+ stem cell
Vili
Crypt
Wnt Ligand
Negative regulators
Positive regulators
TA zone
ISC zone
AIMP2
RNF43...
LGR4, LRP6...
LGR5
Wnt
LRP
Frizzled
DVL
AXIN
APC
β-CATENIN
GSK3β
AIMP2
TCF

MATERIALS AND METOHDS

Mice

The *Apc*$^{Min/+}$ and the *Lgr5-EGFP-IRES-CreERT2* (*Lgr5-EGFP*) mice were purchased from Jackson Laboratories. The generation of *Aimp2* mutant mice has been described elsewhere (Kim et al., 2002). The *Aimp2* mutant mice had been backcrossed at least eight times onto the C57BL/6J backgrounds. *Apc*$^{Min/+}$ mice were interbred with *Aimp2*$^{+/-}$ mice to generate *Aimp2*$^{+/+}$*:Apc*$^{Min/+}$ and *Aimp2*$^{+/-}$*:Apc*$^{Min/+}$ littermates. All animal experiments were performed in accordance with the guidelines of Seoul National University Institutional Animal Care and Use Committee.

Histopathological analysis

For assessment of polyposis in *Apc*$^{Min/+}$ mice, Intestine segments were subdivided into four segments (duodenum, jejunum, ileum and colon), flushed with PBS and opened longitudinally onto 3MM paper or embedded in paraffin wax. The tissues were fixed overnight at 4 ℃ in 4% paraformaldehyde. Adenomas were stained with methylene blue and analyzed with the aid of dissecting microscope (Zeiss). For detailed histological analysis, sections were stained with Hematoxyline & Eosin (H&E) or Periodic acid–Schiff (PAS)/Hematoxylin (H).

Immunofluorescence

For histological analysis, tissues were fixed in 4% paraformaldehyde overnight at 4℃ and embedded in paraffin wax for sectioning. The sections (4 μm) were stained with hematoxylin and eosin (H&E) or Periodic acid–Schiff (PAS)/Hematoxylin (H). For immunohistochemistry, paraffin-embedded sections were rehydrated, and the antigenic epitopes were exposed using Tris/ethylenediaminetetraacetic acid (EDTA) buffer. Sections were incubated in blocking solution (5% BSA, 5% goat serum or horse serum, and 0.5% Tween-20 in PBS) at room temperature for 4 hr and then incubated with primary antibodies to AIMP2 (1:200; Proteintech), BrdU (1:200; Abcam), Ki67 (1:200; Leica Biosystems), GFP (1:200; Abcam), chromogranin A (1:200; Santa Cruz), lysozyme (1:200; DAKO), cleaved Caspase 3 (1:200; Cell signaling) and CD44 (1:200; BD Biosciences). Cell death was assessed by TdT-mediated dUTP nick end labelling (TUNEL) of paraffin-embedded sections of the respective genotypes using the TUNEL cell death detection kit (Roche). For immunocytochemistry, HCT116 cells plated on cover slides washed with PBS at room temperature, fixed in 4% paraformaldehyde for 60 minutes, and blocked with 5% BSA in PBS at room temperature for 4 hr. Samples were incubated with primary antibodies to HA (Santa Cruz) and GFP (Abcam) overnight at 4℃. Specific binding was detected with an Alexa 488-conjugated (green) and/or Alexa 594-conjugated (red) antibody (Molecular Probes). Immunofluorescence was detected using an Observer Z1 fluorescent microscope (Zeiss) equipped with a SPOT Flex camera or with an

LSM710 confocal system (Zeiss).

Intestinal epithelium and crypt isolation

The small intestine was removed, and the fat/mesentery was dissected away. After a flush with cold PBS, a fragment (4 cm) of the ileum from *Aimp2* mutant or control littermates was rinsed again with cold PBS. The fragments were cut into 3- to 5-mm pieces and placed into 50-ml conical tubes that were then filled with 30 ml of cold PBS containing 20 mM EDTA. The samples were incubated for 30 min at 4℃ with intermittent shaking. The samples were then washed with 10 ml of cold PBS. The first supernatant consisted of debris and a few villi. The second to fifth supernatants contained the majority of the intestinal epithelium, including the villi and crypts. The isolated intestinal epithelium was centrifuged 200 × *g* for 5 min at 4℃ to separate the villi and crypts from single cells, and the resulting pellets were used for immunoblotting and qRT-PCR analysis. For villus fraction, the second and third supernatants were centrifuged at 200 × *g* for 5 min and used for qRT-PCR analysis. For crypt isolation, the fourth and fifth supernatants were passed through a 70-μm cell strainer (BD Biosciences) to remove residual villous material. Isolated crypts were centrifuged at 200 × *g* for 5 min and used for qRT-PCR analysis and organoid culture.

Cell culture and *in vitro* reporter assay

All cell lines were obtained from the American Type Culture Collection (ATCC, 2015). Upon

receipt, cells were frozen, and individual aliquots were taken into culture, for analysis within <10 passages. HCT116, HeLa, HEK and MEF cells were cultured in medium (HCT116: RPMI 1640, HeLa, HEK and MEF: DMEM) supplemented with 10% FBS (HyClone Labs), 100 U/ml penicillin, and 100 μg/ml streptomycin in an atmosphere of 95% air and 5% CO_2 at 37℃. ATCC checks the authenticity of these cell lines using short tandem repeat analyses. For reporter assays, cells were transfected with the indicated plasmids. siRNA to *AIMP2* was designed and synthesized by Dharmacon (Thermo Scientific). Luciferase activity was measured using the Dual Luciferase Reporter Assay Kit (Promega).

Co-immunoprecipitation

Co-immunoprecipitation was performed as described previously (Choi et al., 2009a). The cells were lysed in protein lysis buffer (0.1% NP-40, 25 mM Tris, 0.5 mM EGTA, 10 mM NaCl, 0.5 mM $MgCl_2$, 1 mM EDTA, proteinase/phosphatase inhibitor cocktail). The lysates were centrifuged at 12,000 rpm for 30 min. The supernatants were immunoprecipitated for overnight at 4℃ with a normal IgG antibody (Santa Cruz) or a specific monoclonal antibody which is pre-incubated with Protein A/G agarose beads. Beads were washed 6 times with cold protein lysis buffer. The precipitates were separated by SDS-PAGE. After the proteins were transferred to a PVDF membrane, co-immunoprecipitation was assessed by immunoblotting.

Dose-reponse curve analysis

All curve fitting was done in GraphPad Prism. Each point shown in Wnt3a dose-response curve assay represents the mean of measurements from triplicate wells, with error bars representing the SEM. The experiment was repeated at least three times. The solid lines represent nonlinear curve fits of the data to a sigmoidal (variable-slope) equation. Curve fits were calculated in GraphPad Prism using the log (agonist) versus response or normalized response as appropriate.

Immunoblotting and qRT-PCR analysis

Immunoblotting was performed as described previously (Kim et al., 2012a). Primary antibodies to AIMP2 (Proteintech), active β-catenin (Upstate), AXIN2 (Abcam), NKD1 (Abcam), DVL1 (Santa Cruz), TRAF2 (Santa Cruz), p53 (Cell Signaling), phospho-p53 (ser15) (Cell Signaling), anti-GFP (Abcam), anti-HA (Santa Cruz), anti-Myc (Cell Signaling) and β-actin (Sigma) were utilized to detect each protein. Protein bands were detected with enhanced chemiluminescence (Amersham Pharmacia Biotech), and analyzed by ImageJ software (NIH). For qRT-PCR analysis, total RNA was isolated from samples using TRIzol reagent (Life Technologies), and complementary DNA synthesis was performed according to the manufacturer's instructions (Omniscript kit; Qiagen). The data were normalized to β-actin.

qRT-PCR primer information

Actin: 5'- AAGGAAGGCTGGAAAAGAGC -3' 5'- AAATCGTGCGTGACATCAAA -3'

Bmp2: 5’-GAAGTTCCTCCACGGCTTCT-3’ 5’-AGATCTGTACCGCAGGCACT-3’

Smad6: 5’- GTGCTCCCAGTACGCCAC -3’ 5’- ACCAACTCCCTCATCACTGC -3’

Ephb3: 5’- AAGAGACTCTCATGGACACGAAAT-3’ 5’-ACTTCCCGCCGCCAGATG-3’

Sox9: 5’- CGGCGGACCCTGAGATTGC -3’ 5’-CTGGAGGCTGCTGAACGAGAG -3’

Aimp2: 5’-GGTTTGCGTTGATCACAATG-3’ 5’-AGTTGAAGGCAGCAGTCGAT-3’

Gob5: 5’- TCTTGTGTAGATGCCATCATTTTT -3’ 5’- CCAATGTCACAGCCCTCATA -3’

Chga: 5’- GTCTCCAGACACTCAGGGCT -3’ 5’- ATGACAAAAGGGGACACCAA -3’

Mmp7: 5’- CAGACTTACCTCGGATCGTAGTGG-3’

5’- GTTCACTCCTGCGTCCTCACC-3’

Lyz: 5’-ATGGAATGGCTGGCTACTATGGAG-3’

5’-CTCACCACCCTCTTTGCACATTG-3’

Lgr5: 5’-GAGTCAACCCAAGCCTTAGT-3’ 5’-CATGGGACAAATGCAACTGA-3’

Olfm4: 5’- GCCACTTTCCAATTTCAC-3’ 5’- GAGCCTCTTCTCATACAC-3’

Msi1: 5’-GATGCCTTCATGCTGGGTAT-3’ 5’-AATTCGGGGAACTGGTAGGT-3’

C-myc: 5’-ACGGAGTCGTAGTCGAGGTC-3’ 5’-AGAGCTCCTCGAGCTGTTTG-3’

Cd44: 5’-TCCACATGGAATACACCTGC-3’ 5’-CAAGTTTTGGTGGCACACAG-3’

Axin2: 5’-TGCATCTCTCTCTGGAGCTG-3’ 5’-ACAGCGAGTTATCCAGCGAC-3’

Nkd1: 5’-GTAATGTCCTCACGGGTCACTT-3’ 5’- AGAATGGAGAGACTGAGCGAAC -3’

Puma: 5’-TGTCGATGCTGCTCTTCTTG-3’ 5’-GTGTGGAGGAGGAGGAGTGG-3’

Perp; 5’-GGCGAAGAACGAGAGAATGAA-3’ 5’-GCTGCAGCCACGCTTTTC-3’

Bax; 5’- CCCCAGTTGAAGTTGCCATC-3’ 5’-GTTTCATCCAGGATCGAGCAG-3’

Tnfa: 5’-ACCCTGGTATGAGCCCATATAC-3’ 5’-ACACCCATTCCCTTCACAGAG-3’

A20: 5’-GTTGTCCCATTCGTCATTCC-3’ 5’-AAACCAATGGTGATGGAAACTG-3’

Ikba: 5’-GCCACTTTCCACTTATAATGTC-3’ 5’-GTAACCTACCAAGGCTACTC-3’

AXIN2: 5’-CAAACTCATCGCTTGCTTTTT-3’ 5’-CACTTACTTTTTCTGTGGGGAAG-3’

NKD1: 5’- GCTGAGCGTGTCTCTCAACA -3’ 5’- AGGAGTGGATCGGGAGACAG -3’

Organoid culture

Freshly isolated crypts were pelleted and mixed with 30 µl of Matrigel (BD Biosciences). After Matrigel polymerization, advanced DMEM/F12 (Invitrogen) containing 50 ng/ml EGF (Peprotech), 250 ng/ml R-spondin 1 (R&D systems), and 100 ng/ml Noggin (Peprotech) was

added. After culture for 7 days, organoids were removed from the Matrigel, dissociated mechanically, and transferred into fresh Matrigel and medium (split ratio 1:6) under the indicated growth conditions. Growth of the organoids was measured daily using stereomicroscopy, and the formation of organoids was scored. The proliferation rate was determined by counting the number of BrdU-positive vs. DAPI-positive cells. The organoids were incubated with 20 μM BrdU for 1 hr at 37℃ before fixation. For organoid size measurement, morphometric software (INS Industry), SPOT software (version 5.1; Diagnostic Instruments), and Photoshop CS6 (Adobe) were used.

Statistical analysis

Statistical significance was determined by applying Student *t*-test or analysis of variance (ANOVA) to raw values from at least 3 independent experiments. ANOVA was used to evaluate the dependence of a parameter on *Aimp2* gene dosage. Data are as the mean ± standard error of the mean (SEM). *$P < 0.01$ was considered statistically significant.

REFERENCES

Andreu, P., Colnot, S., Godard, C., Gad, S., Chafey, P., Niwa-Kawakita, M., Laurent-Puig, P., Kahn, A., Robine, S., Perret, C., and Romagnolo, B. (2005). Crypt-restricted proliferation and commitment to the Paneth cell lineage following Apc loss in the mouse intestine. Development *132*, 1443-1451.

Aoki, K., Tamai, Y., Horiike, S., Oshima, M., and Taketo, M. M. (2003). Colonic polyposis caused by mTOR-mediated chromosomal instability in Apc+/Delta716 Cdx2+/- compound mutant mice. Nature genetics *35*, 323-330.

Artavanis-Tsakonas, S., Rand, M. D., and Lake, R. J. (1999). Notch signaling: cell fate control and signal integration in development. Science *284*, 770-776.

Barker, N., Ridgway, R. A., van Es, J. H., van de Wetering, M., Begthel, H., van den Born, M., Danenberg, E., Clarke, A. R., Sansom, O. J., and Clevers, H. (2009). Crypt stem cells as the cells-of-origin of intestinal cancer. Nature *457*, 608-611.

Barker, N., van de Wetering, M., and Clevers, H. (2008). The intestinal stem cell. Genes & development *22*, 1856-1864.

Barker, N., van Es, J. H., Kuipers, J., Kujala, P., van den Born, M., Cozijnsen, M., Haegebarth, A., Korving, J., Begthel, H., Peters, P. J., and Clevers, H. (2007). Identification of stem cells in small intestine and colon by marker gene Lgr5. Nature *449*, 1003-1007.

Brady, C. A., Jiang, D., Mello, S. S., Johnson, T. M., Jarvis, L. A., Kozak, M. M., Kenzelmann Broz, D., Basak, S., Park, E. J., McLaughlin, M. E.*, et al.* (2011). Distinct p53 transcriptional

programs dictate acute DNA-damage responses and tumor suppression. Cell *145*, 571-583.

Buczacki, S. J., Zecchini, H. I., Nicholson, A. M., Russell, R., Vermeulen, L., Kemp, R., and Winton, D. J. (2013). Intestinal label-retaining cells are secretory precursors expressing Lgr5. Nature *495*, 65-69.

Cadigan, K. M., and Peifer, M. (2009). Wnt signaling from development to disease: insights from model systems. Cold Spring Harbor perspectives in biology *1*, a002881.

Chen, B., Dodge, M. E., Tang, W., Lu, J., Ma, Z., Fan, C. W., Wei, S., Hao, W., Kilgore, J., Williams, N. S.*, et al.* (2009). Small molecule-mediated disruption of Wnt-dependent signaling in tissue regeneration and cancer. Nature chemical biology *5*, 100-107.

Choi, J. W., Kim, D. G., Park, M. C., Um, J. Y., Han, J. M., Park, S. G., Choi, E. C., and Kim, S. (2009a). AIMP2 promotes TNFalpha-dependent apoptosis via ubiquitin-mediated degradation of TRAF2. Journal of cell science *122*, 2710-2715.

Choi, J. W., Um, J. Y., Kundu, J. K., Surh, Y. J., and Kim, S. (2009b). Multidirectional tumor-suppressive activity of AIMP2/p38 and the enhanced susceptibility of AIMP2 heterozygous mice to carcinogenesis. Carcinogenesis *30*, 1638-1644.

Clevers, H. (2006). Wnt/beta-catenin signaling in development and disease. Cell *127*, 469-480.

Clevers, H., and Nusse, R. (2012). Wnt/beta-catenin signaling and disease. Cell *149*, 1192-1205.

Clevers, H. C., and Bevins, C. L. (2013). Paneth cells: maestros of the small intestinal crypts. Annual review of physiology *75*, 289-311.

de Lau, W., Peng, W. C., Gros, P., and Clevers, H. (2014). The R-spondin/Lgr5/Rnf43 module: regulator of Wnt signal strength. Genes & development *28*, 305-316.

Farin, H. F., Van Es, J. H., and Clevers, H. (2012). Redundant sources of Wnt regulate intestinal stem cells and promote formation of Paneth cells. Gastroenterology *143*, 1518-1529 e1517.

Fearon, E. R., and Vogelstein, B. (1990). A genetic model for colorectal tumorigenesis. Cell *61*, 759-767.

Fodde, R., Edelmann, W., Yang, K., van Leeuwen, C., Carlson, C., Renault, B., Breukel, C., Alt, E., Lipkin, M., Khan, P. M., and et al. (1994). A targeted chain-termination mutation in the mouse Apc gene results in multiple intestinal tumors. Proceedings of the National Academy of Sciences of the United States of America *91*, 8969-8973.

Groden, J., Thliveris, A., Samowitz, W., Carlson, M., Gelbert, L., Albertsen, H., Joslyn, G., Stevens, J., Spirio, L., Robertson, M., and et al. (1991). Identification and characterization of the familial adenomatous polyposis coli gene. Cell *66*, 589-600.

Guma, M., Stepniak, D., Shaked, H., Spehlmann, M. E., Shenouda, S., Cheroutre, H., Vicente-Suarez, I., Eckmann, L., Kagnoff, M. F., and Karin, M. (2011). Constitutive intestinal NF-kappaB does not trigger destructive inflammation unless accompanied by MAPK activation. The Journal of experimental medicine *208*, 1889-1900.

Haigis, K. M., Caya, J. G., Reichelderfer, M., and Dove, W. F. (2002). Intestinal adenomas can develop with a stable karyotype and stable microsatellites. Proceedings of the National Academy of Sciences of the United States of America *99*, 8927-8931.

Han, J. M., Park, B. J., Park, S. G., Oh, Y. S., Choi, S. J., Lee, S. W., Hwang, S. K., Chang, S. H., Cho, M. H., and Kim, S. (2008). AIMP2/p38, the scaffold for the multi-tRNA synthetase complex, responds to genotoxic stresses via p53. Proceedings of the National Academy of Sciences of the United States of America *105*, 11206-11211.

He, X. C., Zhang, J., Tong, W. G., Tawfik, O., Ross, J., Scoville, D. H., Tian, Q., Zeng, X., He, X., Wiedemann, L. M.*, et al.* (2004). BMP signaling inhibits intestinal stem cell self-renewal through suppression of Wnt-beta-catenin signaling. Nature genetics *36*, 1117-1121.

Ireland, H., Kemp, R., Houghton, C., Howard, L., Clarke, A. R., Sansom, O. J., and Winton, D. J. (2004). Inducible Cre-mediated control of gene expression in the murine gastrointestinal tract: effect of loss of beta-catenin. Gastroenterology *126*, 1236-1246.

Kim, H. A., Koo, B. K., Cho, J. H., Kim, Y. Y., Seong, J., Chang, H. J., Oh, Y. M., Stange, D. E., Park, J. G., Hwang, D., and Kong, Y. Y. (2012a). Notch1 counteracts WNT/beta-catenin signaling through chromatin modification in colorectal cancer. The Journal of clinical investigation *122*, 3248-3259.

Kim, J. Y., Kang, Y. S., Lee, J. W., Kim, H. J., Ahn, Y. H., Park, H., Ko, Y. G., and Kim, S. (2002). p38 is essential for the assembly and stability of macromolecular tRNA synthetase complex: implications for its physiological significance. Proceedings of the National Academy of Sciences of the United States of America *99*, 7912-7916.

Kim, M. J., Park, B. J., Kang, Y. S., Kim, H. J., Park, J. H., Kang, J. W., Lee, S. W., Han, J. M., Lee, H. W., and Kim, S. (2003). Downregulation of FUSE-binding protein and c-myc by tRNA synthetase cofactor p38 is required for lung cell differentiation. Nature genetics *34*,

330-336.

Kim, S., You, S., and Hwang, D. (2011). Aminoacyl-tRNA synthetases and tumorigenesis: more than housekeeping. Nature reviews Cancer *11*, 708-718.

Kim, T. H., Escudero, S., and Shivdasani, R. A. (2012b). Intact function of Lgr5 receptor-expressing intestinal stem cells in the absence of Paneth cells. Proceedings of the National Academy of Sciences of the United States of America *109*, 3932-3937.

Kishida, S., Yamamoto, H., Hino, S., Ikeda, S., Kishida, M., and Kikuchi, A. (1999). DIX domains of Dvl and axin are necessary for protein interactions and their ability to regulate beta-catenin stability. Molecular and cellular biology *19*, 4414-4422.

Ko, H. S., Lee, Y., Shin, J. H., Karuppagounder, S. S., Gadad, B. S., Koleske, A. J., Pletnikova, O., Troncoso, J. C., Dawson, V. L., and Dawson, T. M. (2010). Phosphorylation by the c-Abl protein tyrosine kinase inhibits parkin's ubiquitination and protective function. Proceedings of the National Academy of Sciences of the United States of America *107*, 16691-16696.

Ko, H. S., von Coelln, R., Sriram, S. R., Kim, S. W., Chung, K. K., Pletnikova, O., Troncoso, J., Johnson, B., Saffary, R., Goh, E. L.*, et al.* (2005). Accumulation of the authentic parkin substrate aminoacyl-tRNA synthetase cofactor, p38/JTV-1, leads to catecholaminergic cell death. The Journal of neuroscience : the official journal of the Society for Neuroscience *25*, 7968-7978.

Ko, Y. G., Park, H., Kim, T., Lee, J. W., Park, S. G., Seol, W., Kim, J. E., Lee, W. H., Kim, S. H., Park, J. E., and Kim, S. (2001). A cofactor of tRNA synthetase, p43, is secreted to up-

regulate proinflammatory genes. The Journal of biological chemistry *276*, 23028-23033.

Koo, B. K., Spit, M., Jordens, I., Low, T. Y., Stange, D. E., van de Wetering, M., van Es, J. H., Mohammed, S., Heck, A. J., Maurice, M. M., and Clevers, H. (2012). Tumour suppressor RNF43 is a stem-cell E3 ligase that induces endocytosis of Wnt receptors. Nature *488*, 665-669.

Korinek, V., Barker, N., Moerer, P., van Donselaar, E., Huls, G., Peters, P. J., and Clevers, H. (1998). Depletion of epithelial stem-cell compartments in the small intestine of mice lacking Tcf-4. Nature genetics *19*, 379-383.

Lee, Y., Karuppagounder, S. S., Shin, J. H., Lee, Y. I., Ko, H. S., Swing, D., Jiang, H., Kang, S. U., Lee, B. D., Kang, H. C.*, et al.* (2013). Parthanatos mediates AIMP2-activated age-dependent dopaminergic neuronal loss. Nature neuroscience *16*, 1392-1400.

Logan, C. Y., and Nusse, R. (2004). The Wnt signaling pathway in development and disease. Annual review of cell and developmental biology *20*, 781-810.

Moser, A. R., Pitot, H. C., and Dove, W. F. (1990). A dominant mutation that predisposes to multiple intestinal neoplasia in the mouse. Science *247*, 322-324.

Munoz, J., Stange, D. E., Schepers, A. G., van de Wetering, M., Koo, B. K., Itzkovitz, S., Volckmann, R., Kung, K. S., Koster, J., Radulescu, S.*, et al.* (2012). The Lgr5 intestinal stem cell signature: robust expression of proposed quiescent '+4' cell markers. The EMBO journal *31*, 3079-3091.

Park, B. J., Kang, J. W., Lee, S. W., Choi, S. J., Shin, Y. K., Ahn, Y. H., Choi, Y. H., Choi, D., Lee, K. S., and Kim, S. (2005a). The haploinsufficient tumor suppressor p18 upregulates p53

via interactions with ATM/ATR. Cell *120*, 209-221.

Park, S. G., Ewalt, K. L., and Kim, S. (2005b). Functional expansion of aminoacyl-tRNA synthetases and their interacting factors: new perspectives on housekeepers. Trends in biochemical sciences *30*, 569-574.

Pinto, D., Gregorieff, A., Begthel, H., and Clevers, H. (2003). Canonical Wnt signals are essential for homeostasis of the intestinal epithelium. Genes & development *17*, 1709-1713.

Quevillon, S., Robinson, J. C., Berthonneau, E., Siatecka, M., and Mirande, M. (1999). Macromolecular assemblage of aminoacyl-tRNA synthetases: identification of protein-protein interactions and characterization of a core protein. Journal of molecular biology *285*, 183-195.

San Roman, A. K., Jayewickreme, C. D., Murtaugh, L. C., and Shivdasani, R. A. (2014). Wnt secretion from epithelial cells and subepithelial myofibroblasts is not required in the mouse intestinal stem cell niche in vivo. Stem cell reports *2*, 127-134.

Sangiorgi, E., and Capecchi, M. R. (2008). Bmi1 is expressed in vivo in intestinal stem cells. Nature genetics *40*, 915-920.

Sato, T., van Es, J. H., Snippert, H. J., Stange, D. E., Vries, R. G., van den Born, M., Barker, N., Shroyer, N. F., van de Wetering, M., and Clevers, H. (2011). Paneth cells constitute the niche for Lgr5 stem cells in intestinal crypts. Nature *469*, 415-418.

Sato, T., Vries, R. G., Snippert, H. J., van de Wetering, M., Barker, N., Stange, D. E., van Es, J. H., Abo, A., Kujala, P., Peters, P. J., and Clevers, H. (2009). Single Lgr5 stem cells build crypt-villus structures in vitro without a mesenchymal niche. Nature *459*, 262-265.

Schwarz-Romond, T., Fiedler, M., Shibata, N., Butler, P. J., Kikuchi, A., Higuchi, Y., and Bienz, M. (2007). The DIX domain of Dishevelled confers Wnt signaling by dynamic polymerization. Nature structural & molecular biology *14*, 484-492.

Takayama, T., Katsuki, S., Takahashi, Y., Ohi, M., Nojiri, S., Sakamaki, S., Kato, J., Kogawa, K., Miyake, H., and Niitsu, Y. (1998). Aberrant crypt foci of the colon as precursors of adenoma and cancer. The New England journal of medicine *339*, 1277-1284.

van de Wetering, M., Sancho, E., Verweij, C., de Lau, W., Oving, I., Hurlstone, A., van der Horn, K., Batlle, E., Coudreuse, D., Haramis, A. P.*, et al.* (2002). The beta-catenin/TCF-4 complex imposes a crypt progenitor phenotype on colorectal cancer cells. Cell *111*, 241-250.

van der Flier, L. G., and Clevers, H. (2009). Stem cells, self-renewal, and differentiation in the intestinal epithelium. Annual review of physiology *71*, 241-260.

van der Flier, L. G., van Gijn, M. E., Hatzis, P., Kujala, P., Haegebarth, A., Stange, D. E., Begthel, H., van den Born, M., Guryev, V., Oving, I.*, et al.* (2009). Transcription factor achaete scute-like 2 controls intestinal stem cell fate. Cell *136*, 903-912.

van Es, J. H., Sato, T., van de Wetering, M., Lyubimova, A., Nee, A. N., Gregorieff, A., Sasaki, N., Zeinstra, L., van den Born, M., Korving, J.*, et al.* (2012). Dll1+ secretory progenitor cells revert to stem cells upon crypt damage. Nature cell biology *14*, 1099-1104.

van Es, J. H., van Gijn, M. E., Riccio, O., van den Born, M., Vooijs, M., Begthel, H., Cozijnsen, M., Robine, S., Winton, D. J., Radtke, F., and Clevers, H. (2005). Notch/gamma-secretase inhibition turns proliferative cells in intestinal crypts and adenomas into goblet cells. Nature *435*, 959-963.

Wakasugi, K., Slike, B. M., Hood, J., Ewalt, K. L., Cheresh, D. A., and Schimmel, P. (2002). Induction of angiogenesis by a fragment of human tyrosyl-tRNA synthetase. The Journal of biological chemistry *277*, 20124-20126.

Wu, H. (2013). Higher-order assemblies in a new paradigm of signal transduction. Cell *153*, 287-292.

Zhang, J., and Chen, Q. M. (2013). Far upstream element binding protein 1: a commander of transcription, translation and beyond. Oncogene *32*, 2907-2916.

국문초록

장 내 항상성 및 암 형성에서의 AIMP2 의 기능 연구

Wnt/β-catenin (CTNNB1) 신호는 장 상피 줄기세포의 증식과 유지에 매우 중요한 역할을 담당한다. Wnt/β-catenin (CTNNB1) 신호가 없는 경우 장 상피 줄기세포는 즉각적인 세포 사멸을 겪고 장 크립트가 파괴된다. 장 상피 줄기세포는 크립트 안에서 파네스 세포 (Paneth cell) 및 크립트 간충직 세포 (Cryptal mesenchymal cell) 등에 의해 이루어진 미세환경으로부터 풍부한 Wnt 리간드를 지속적으로 공급 받는다. 하지만 Wnt/β-catenin 신호의 과도한 활성화는 장 상피 줄기세포의 확장과 더불어 대장암을 유발하므로 적절한 수준의 Wnt/β-catenin 신호 수준을 유지하기 위해서는 Wnt/β-catenin 신호의 음성조절자가 반드시 필요하다.

대장암은 세계에서 세 번째로 흔한 암이며 암 관련 사망의 두 번째 주요 원인이다. 대장암의 조기 진단은 치료를 가능케 하지만 조기 진단의 가능성을

높이려면 대장암의 초기 증상을 이해하는 것이 매우 중요하다. 장 상피 줄기세포는 대장암의 기원이 되는 세포이며 종양 형성의 초기단계에 장 상피 줄기세포의 확장이 일어난다는 것이 알려져 있다. 따라서 장 상피 줄기세포 구획의 크기와 종양 발생률을 제어하는 분자 메커니즘을 이해하는 것이 필수적이다.

Aminoacyl-tRNA synthetase interacting multifunctional proteins (AIMPs) 는 단백질 생산에 관여하는 단백질로 처음 동정되었으며 특정 아미노산을 tRNA에 부착시켜주는 아미노산-tRNA 중합효소 복합체를 안정화 시키는 기능을 수행한다. 최근 AIMP는 아미노-아실화에서의 기능뿐 아니라 혈관형성, 면역반응, 세포사멸 등에 영향을 미치는 신호체계에도 관여한다는 것이 밝혀지고 있다. 또한 이 AIMP 들이 암과 관련된 신호체계에도 연관되어 있음이 보고되고 있다.

본 연구에서는 대장암 생쥐모델을 활용하여 AIMP2와 Wnt/β-catenin 신호체계의 관련성을 장 상피 항상성 유지의 관점에서 밝혀보고자 한다. *Aimp2* 유전자의 반성접합성 결실은 장 상피에서 Wnt/β-catenin 신호의 활성화를 유발하고 크립트 내 세포증식과 장 상피 줄기세포 구획을 확장시킨다. $Apc^{Min/+}$

생쥐와의 교배 결과 AIMP2의 감소는 선종의 발생을 증가시켰다. AIMP2는 Dishevelled에 결합하여 AXIN과 Dishevelled의 상호작용을 저해함으로써 Wnt/β-catenin 신호를 억제하며, 장 상피 Organoid의 형성과 성장을 *Aimp2*-유전자량 의존적으로 저해하였다. 종합해보면, 우리의 결과를 통해서 AIMP2가 장 상피에서 종양 억제자로 작동하며 Wnt/β-catenin 신호 전달을 미세 조정하여 장 상피 줄기세포의 세포밀도와 활성을 조절한다는 것을 알 수 있다.

핵심 단어: 장 상피 항상성; Dishevelled; 대장암; Lgr5; 오가노이드

학번: 2011-20342